



1 **Physical processes in the upwelling regions of the tropical Atlantic**

2

3 Peter Brandt^{1,2}, Gaël Alory³, Founi Mesmin Awo⁴, Marcus Dengler¹, Sandrine Djakouré⁵,
4 Rodrigue Anicet Imbol Koungue¹, Julien Jouanno³, Mareike Körner¹, Marisa Roch¹, Mathieu
5 Rouault⁴

6 ¹GEOMAR Helmholtz Centre for Ocean Research Kiel, Kiel, Germany

7 ²Faculty of Mathematics and Natural Sciences, Kiel University, Kiel, Germany

8 ³LEGOS, CNES/CNRS/IRD/UPS, Toulouse, France

9 ⁴Nansen-Tutu Centre for Marine Environmental Research, Department of Oceanography, University of Cape
10 Town, Cape Town, South Africa

11 ⁵LASMES, UFR SSMT, Felix Houphouët-Boigny University, Abidjan, Côte d'Ivoire

12 *Correspondence to:* Peter Brandt (pbrandt@geomar.de)

13 **Abstract**

14 In this paper, we review observational and modelling results on the upwelling in the inner
15 tropical Atlantic. We focus on the physical processes that drive the seasonal variability of
16 surface cooling and upward nutrient flux required to explain the seasonality of primary
17 productivity. We separately consider the equatorial upwelling system, the northern coastal
18 upwelling system of the Gulf of Guinea and the tropical Angolan upwelling system. For the
19 equatorial regime, we discuss the forcing of upwelling velocity and turbulent mixing as well as
20 the underlying dynamics responsible for thermocline movements and current structure. The
21 coastal upwelling system in the Gulf of Guinea is concentrated along northern boundary and is
22 driven by both, local and remote forcing. The particular role of the Guinea Current, nonlinearity
23 and the shape of the coastline are emphasized. For the tropical Angolan upwelling, we show
24 that this system is not wind-driven, but instead results from the combined effect of coastally
25 trapped waves, surface heat and freshwater fluxes, and turbulent mixing. Finally, we review
26 recent changes in the upwelling systems associated with climate variability and global warming
27 and address possible responses of upwelling systems in future scenarios.

28

29 **Short summary**

30 Tropical upwelling systems are among the most productive ecosystems globally. The tropical
31 Atlantic upwelling undergoes a strong seasonal cycle that is forced by the seasonal cycle of the
32 zonal wind along the equator and the near-coastal wind field off Africa. Besides the wind
33 forcing that lead to an up- and downward movement of the nitracline, turbulent diffusion results
34 in upward mixing of nutrients. Here, we review the different physical processes responsible for
35 upward nutrient supply.

36

37 **1 Introduction**

38

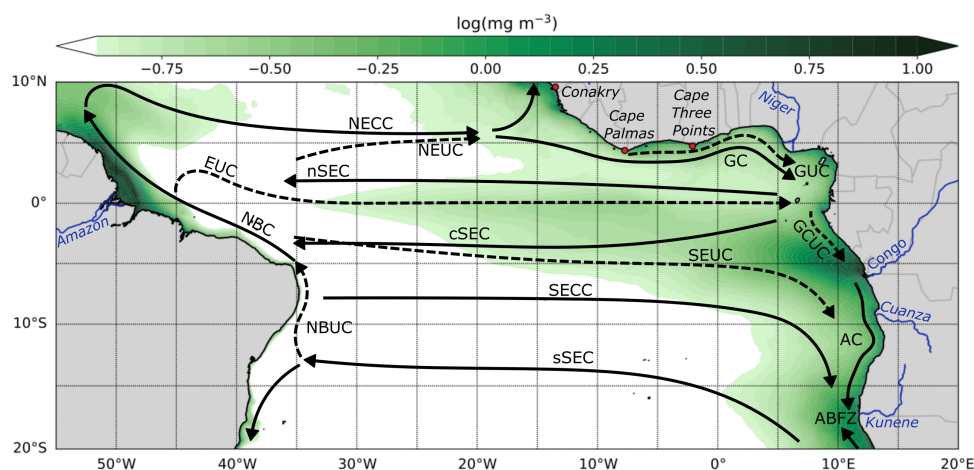
39 The tropical oceans are important to the Earth system for several reasons. The ocean receives a
40 large part of shortwave radiation from the sun arriving at the Earth surface that must be
41 redistributed horizontally and vertically. Similar important exchanges of carbon dioxide,
42 oxygen and other trace gases occur at the interface between tropical ocean and overlying
43 atmosphere. Tropical marine ecosystems are among the most productive ones, with high
44 relevance for global fisheries (Longhurst 1993). They are associated with a substantial carbon
45 flux from the near surface into the deep ocean (Kiko et al. 2017). At the same time, the tropical
46 oceans are affected by modes of natural climate variability that have reverberations around the
47 globe, e.g., including the Pacific El Niño or the Atlantic Niño. Climate warming and change
48 are thought to profoundly affect the tropical oceans. On the one hand, they impact natural
49 climate variability via an intensification of climate extremes or changing of natural variability



50 (Cai et al. 2018; Crespo et al. 2022; Prigent et al. 2020b). On the other hand, they are thought
 51 to enhance stratification thereby impacting subduction, upwelling, and air-sea gas exchange
 52 with consequences for acidification and deoxygenation (Oschlies et al. 2018) and marine
 53 ecosystems.

54 The zonal extend of the tropical Atlantic is similar to that of the Indian Ocean and about three
 55 times smaller than that of the Pacific Ocean. The difference in size between Pacific and Atlantic
 56 oceans seems to be the main reason for the dominance of interannual climate variability in the
 57 tropical Pacific, while the tropical Atlantic has largest variability on seasonal time scales (Burls
 58 et al. 2011; Keenlyside and Latif 2007). A geographical peculiarity of the tropical Atlantic
 59 Ocean is the existence of the Gulf of Guinea which, in addition to its eastern boundary, also has
 60 a northern boundary extending approximately along 5°N from 10°W to 10°E. There are several
 61 major rivers running into the tropical Atlantic including the Amazon, Congo and Niger rivers
 62 (Fig. 1).

63



64

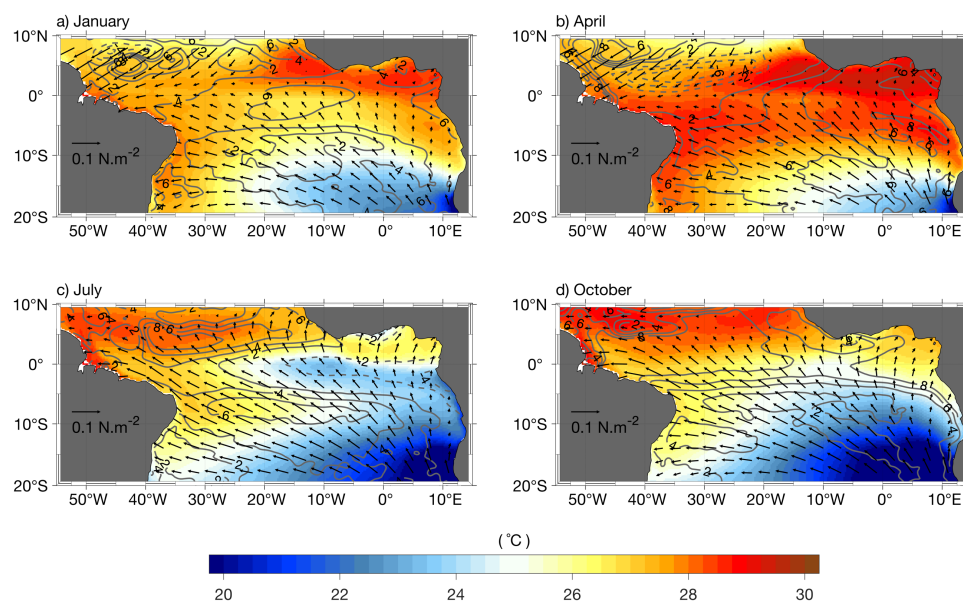
65 **Fig. 1** Mean chlorophyll concentration in the tropical Atlantic with circulation schematic superimposed.
 66 Chlorophyll data are from Copernicus-GlobColour averaged for 1997-2022. Surface (solid arrows) and
 67 thermocline (dashed arrows) current branches shown are the North Equatorial Countercurrent (NECC), the North
 68 Equatorial Undercurrent (NEUC), the Guinea Undercurrent (GUC), the Guinea Current (GC), the North Brazil
 69 Undercurrent (NBUC), the North Brazil Current (NBC), the Equatorial Undercurrent (EUC), the northern,
 70 central and southern branches of the South Equatorial Current (nSEC, cSEC, and sSEC), the South Equatorial
 71 Undercurrent (SEUC), the South Equatorial Countercurrent (SECC), the Gabon-Congo Undercurrent (GCUC),
 72 and the Angola Current (AC). Also marked is the Angola-Benguela Frontal Zone (ABFZ) at about 17°S and the
 73 rivers Amazon, Niger, Congo, Cuanza, and Kunene.

74

75 Based on satellite data, Longhurst (1993) provided a first systematic overview of the different
 76 open ocean and coastal upwelling systems in the tropical Atlantic. Today, mean satellite
 77 chlorophyll concentration (Fig. 1) reveals strongly enhanced productivity in the region of the
 78 Amazon River and the Congo River mouths. In the region of the Niger River mouth no
 79 comparable signal of enhanced productivity is found likely due to its much-reduced discharge
 80 (Fig. 1). Besides the impact of river discharge on the mean chlorophyll concentration, high
 81 productivity is found near the coasts in the Gulf of Guinea upwelling system (GGUS), and the
 82 tropical Angolan upwelling system (tAUS). The equatorial Atlantic upwelling system (EAUS)
 83 is instead characterized by albeit enhanced but in comparison to the coastal upwelling systems
 84 relatively weak chlorophyll concentration (note the logarithmic scale for the chlorophyll
 85 concentration in Fig. 1) (Grotsky et al. 2008). Nevertheless, the EAUS is still of major
 86 importance for the overall productivity in the tropical Atlantic due to the large oceanic area
 87 covered.



88 Upwelling in the eastern tropical Atlantic is supplied by thermocline waters transported in
89 different eastward currents. Tropical Atlantic upwelling is an element of the shallow
90 overturning circulation, the subtropical cells (STCs), and is connected to the subduction in the
91 eastern subtropics via equatorward thermocline flow and poleward Ekman transport in the
92 surface layer (Fu et al. 2022; Schott et al. 2004; Tuchen et al. 2020). At the equator, the
93 Equatorial Undercurrent (EUC) transports thermocline waters eastward, toward the EAUS. Due
94 to the presence of the Atlantic meridional overturning circulation, these waters are almost
95 exclusively of southern hemisphere origin (Johns et al. 2014; Schott et al. 1998; Tuchen et al.
96 2022a). Part of the waters recirculates into the westward current branches of the South
97 Equatorial Current, the northern and the central South Equatorial Current, or contributes to
98 supply the southward flow along the eastern boundary within the Gabon-Congo Undercurrent
99 and the Angola Current (Kolodziejczyk et al. 2014; Kopte et al. 2017). The GGUS is supplied
100 by the Guinea Current and the Guinea Undercurrent. While the waters of the Guinea Current
101 mostly originate in the North Equatorial Countercurrent, a similar connection between the
102 North Equatorial Undercurrent and the Guinea Undercurrent is less obvious (Bourlès et al.
103 2002; Djakouré et al. 2017; Herbert et al. 2016).
104 The tropical Atlantic undergoes a strong seasonal cycle associated with the meridional
105 migration of the Intertropical Convergence Zone (Fig. 2). During boreal summer, the
106 Intertropical Convergence Zone migrates northward resulting in strongly enhanced easterly
107 winds along the equator and the establishment of the Atlantic cold tongue (ACT) in the eastern
108 basin centred around 10°W (Fig. 2c). At the eastern boundary between equator and 15°S, the
109 lowest sea surface temperatures (SST) near the coast are found between July and September.
110 At the northern boundary of the Gulf of Guinea, winds strengthen as well during boreal summer
111 in accordance with the development of the West African Monsoon resulting in upwelling
112 favourable westerlies along the Ghanaian coast. Lowest SST near the coast is found in July-
113 August (Fig. 2c). The equatorial Atlantic is warmest in March/April (Fig. 2b) corresponding to
114 a seasonal cycle with a fast cooling during the onset phase of the ACT and slower warming
115 after it has reached its maximum spatial extent (Brandt et al. 2011; Caniaux et al. 2011).
116



117
118 **Fig. 2** Monthly mean sea surface temperature (SST, colour shading), sea level anomaly (contour lines, unit is cm),
119 and wind stress (arrows) during (a) January, (b) April, (c) July and (d) October. SST data are from OI-SST
120 (<https://www.esrl.noaa.gov/psd/data/gridded/>), surface wind stress from ERA5



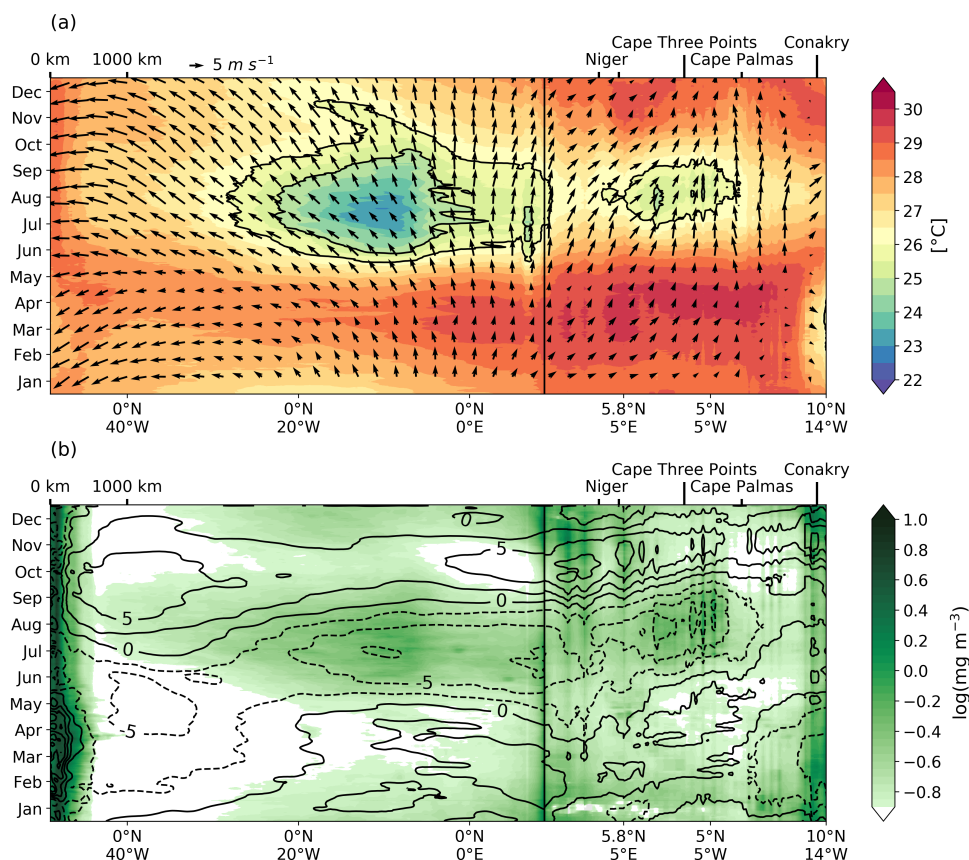
121 (<https://cds.climate.copernicus.eu/>) and sea level anomalies from the European Union Copernicus Marine Service
122 Information (<http://marine.copernicus.eu/>). The data are averaged between 1982-2021.

123

124 In the tropical Atlantic, the thermocline depth often can be associated with the depth of the
125 nitracline. An upward movement of the thermocline thus marks upward vertical advection of
126 nitrate fuelling biological productivity (Radenac et al. 2020). Besides local wind forcing, the
127 propagation of equatorial and coastally trapped waves (CTWs) along the equatorial and coastal
128 waveguides, respectively, contributes to the vertical movement of the thermocline/nitracline.
129 Such wave propagation can result in dynamic upwelling far away from the wave generation
130 sites (Bachelery et al. 2020; Hormann and Brandt 2009; Illig et al. 2018a; Illig et al. 2018b).
131 The Hovmöller diagrams of SST and winds as well as chlorophyll concentration and sea surface
132 height show the seasonal development along the equatorial and coastal waveguides in the
133 northern (Fig. 3) and southern (Fig. 4) hemispheres, respectively. Primary cooling along the
134 equator can be identified following the enhancement of upwelling-favouring easterly winds in
135 May-June (Weingartner and Weisberg 1991). A secondary cooling occurs in November-
136 December (Jouanno et al. 2011a; Okumura and Xie 2006). In the GGUS, where SST reaches
137 minimum values in August (Fig. 3a), upwelling-favouring westerly winds contribute to local
138 cooling (Djakouré et al. 2017). Contrary, the southerly winds in the Angolan upwelling region
139 are particularly weak during phases of coldest sea surface (Fig. 4a) (Körner et al. 2022;
140 Ostrowski et al. 2009). Biological productivity marked by enhanced chlorophyll concentration
141 is generally enhanced during periods of depressed sea surface height or correspondingly during
142 periods of elevated thermocline (Fig. 3b).

143 In this review, we focus on the upper-ocean seasonal cycle in the three eastern-basin upwelling
144 systems of the inner tropical Atlantic, the physical forcing driving the upwelling, the upward
145 nitrate supply, and the resulting biological productivity. Section 2 focusses on equatorial
146 upwelling, section 3 on the Gulf of Guinea coastal upwelling and section 4 on the tropical
147 Angolan upwelling. In section 5, we discuss implications of longer-term changes and global
148 warming for the seasonal cycle, and, finally, in section 6, we provide a conclusion and outlook.

149



150
151
152
153
154
155
156
157
158
159
160
161

Fig. 3 Seasonal cycle of (a) sea surface temperature (shading) and wind stress (arrows) and (b) chlorophyll concentration (shading) and sea level anomaly (contour lines, unit is cm) along the equatorial (left of the vertical black lines) and Gulf of Guinea coastal waveguides (right of the vertical black lines). Marks at the lower x-axis give geographic coordinates and marks at the upper x-axis give a scale for the distance and geographic locations along the waveguides. Also included in (a) are contours of the 25°C and 26°C isotherms to highlight equatorial and coastal upwelling. Positive and negative sea level anomaly in (b) are marked by solid and dashed contour lines, respectively; mean sea level anomaly is removed. SST data are from the Microwave OI SST product averaged for 1998-2022, wind data are from ASCAT and QSCAT averaged for 1991-2021, chlorophyll data are from Copernicus-GlobColour averaged for 1997-2022, sea level anomaly data are from Copernicus DUCAS averaged for 1993-2020.

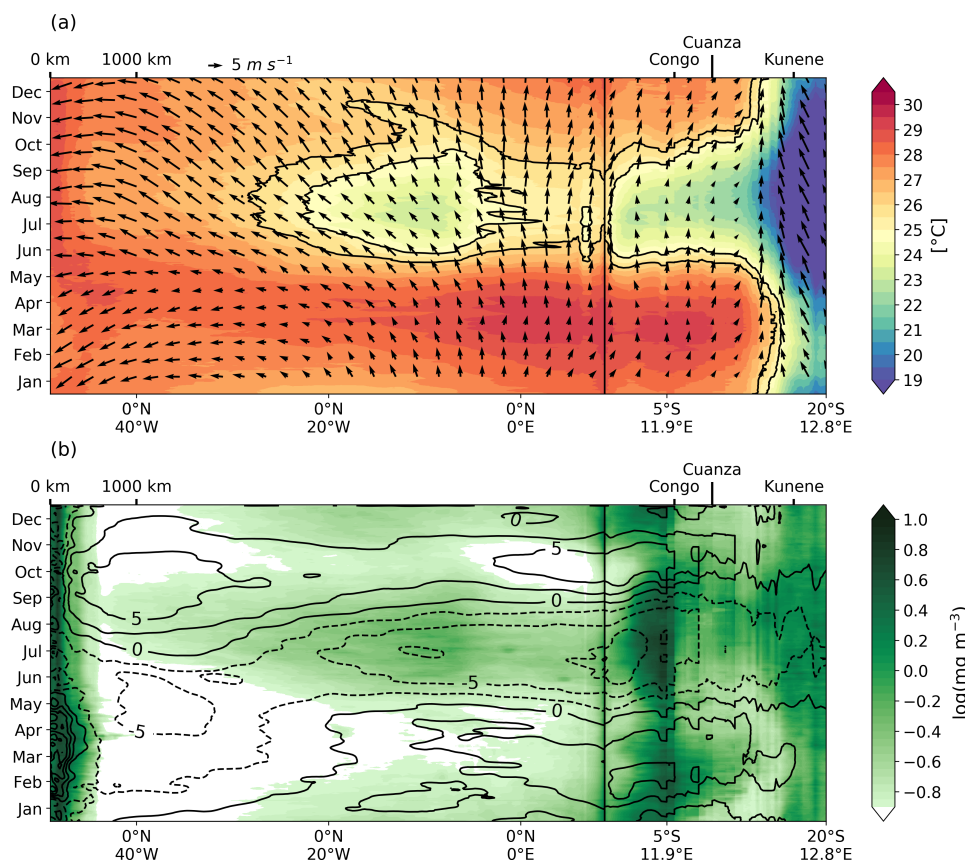


Fig. 4 Same as Fig. 3, but along the southwest African coastal waveguide (right of the vertical black lines).

2 Equatorial upwelling

The equatorial upwelling transports cool, nutrient-rich waters toward the surface of the equatorial Atlantic. Its influence at the surface is more pronounced in the eastern part of the basin, where it gives rise to the development of the ACT. Its intensity is modulated by a seasonal cycle composed of an annual and a semiannual component, with a primary SST minimum in July-August and a secondary minimum in November-December (Fig. 3) (Jouanno et al. 2011a; Okumura and Xie 2006). First insights into the seasonal evolution were obtained from observational studies in the 1980s, revealing a close link between seasonal surface cooling and vertical movements of the thermocline (Merle 1980; Voituriez et al. 1982). Indeed, periods of surface cooling in the eastern equatorial Atlantic (Fig. 3) are in phase with the thermocline upwelling in May-June and November (Fig. 5). By using forced ocean models, Philander and Pacanowski (1981) have revealed variations of the equatorial thermocline as forced by the seasonal cycle of the wind stress: stronger easterlies results in a stronger uplift of the thermocline in the eastern equatorial Atlantic. These authors discussed the response of the Atlantic Ocean to the seasonal wind forcing as an equilibrium response that can be understood as a succession of steady states. However, such an equilibrium response requires the dominance of low baroclinic mode equatorial Kelvin and Rossby waves that propagate fast enough to adjust the thermocline to the wind forcing within the seasonal cycle (Ding et al. 2009; Hormann and Brandt 2009; Philander and Pacanowski 1981; Philander and Pacanowski 1986). Beside

162
163
164
165
166
167
168
169
170
171
172
173
174
175
176
177
178
179
180
181
182
183
184



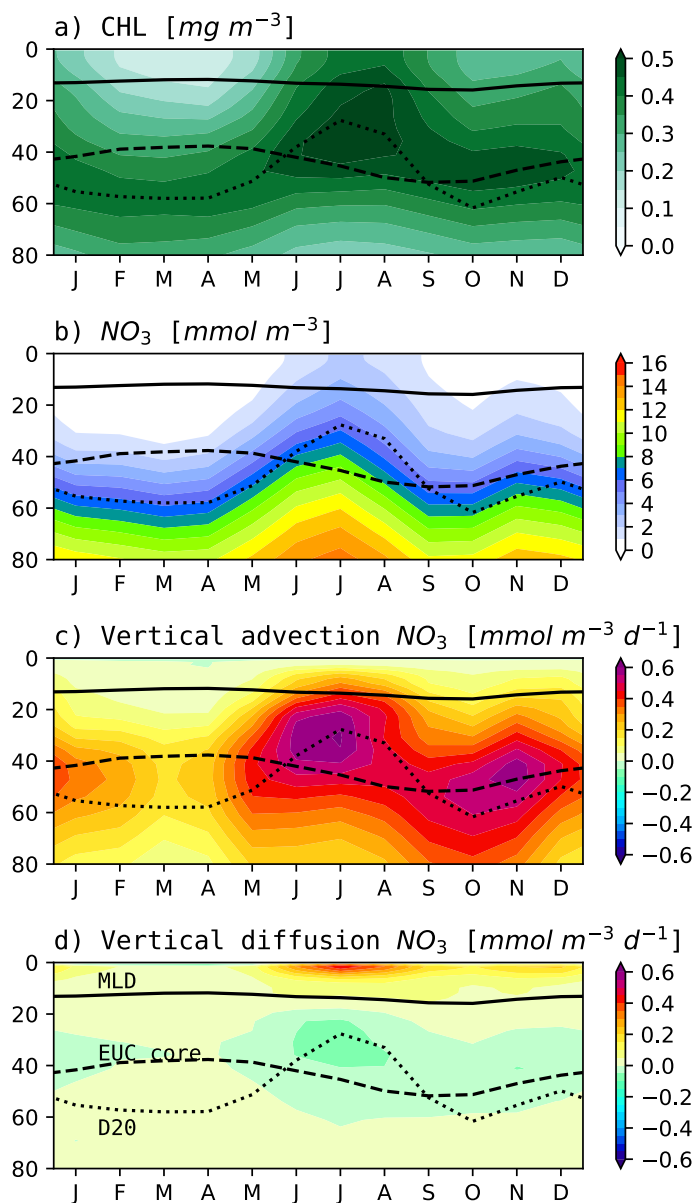
185 the eastern thermocline uplift, the equatorial easterlies force a strong eastward thermocline
186 flow, the EUC, that supplies the upwelling in the eastern equatorial Atlantic (Johns et al. 2014;
187 Schott et al. 1998).

188 The equatorial upwelling is an integral part of the STCs that are driven by the easterlies away
189 from the equator. The equatorial divergence in the Atlantic calculated from the Ekman
190 transports at about 10°S and 10°N, which defines the upwelling transport in the inner tropics,
191 is about 20 Sv (Schott et al. 2004; Tuchen et al. 2019). Easterlies at the equator additionally
192 result in equatorial upwelling that is part of the tropical cells (Perez et al. 2014). Tropical cells
193 are similar overturning circulations as the STCs, but confined only to the upper 100 m with
194 upwelling at the equator and downwelling at about $\pm 3\text{-}5^\circ$ latitude. In the Atlantic the mean
195 tropical cells are found to be asymmetric with respect to the equator; the northern cell extends
196 into the southern hemisphere. This behaviour can be explained by the presence of southerly
197 winds peaking during boreal autumn that drive a cross-equatorial northward surface flow at the
198 equator (Heukamp et al. 2022). This circulation feature, often referred to as the equatorial roll,
199 has maximum southward return flow at about 50 m depth and upwelling and downwelling
200 slightly south and north of the equator, respectively. The different forcing terms of the
201 upwelling velocity in the equatorial Atlantic are numerous and are discussed in detail in
202 Giordani and Caniaux (2011).

203 Over the past decade, several studies have revealed that turbulent mixing helps to define the
204 spatial distribution and temporal variability of equatorial surface cooling (e.g., Jouanno et al.
205 2011a). Turbulent mixing at the base of the mixed layer that drives heat flux out of the mixed
206 layer into the deeper ocean is dominantly induced by the vertical shear of the zonal equatorial
207 currents, that is the westward South Equatorial Current at the surface and the eastward EUC at
208 the thermocline level (Hummels et al. 2013). Different processes such as the seasonal variability
209 in strength and core depth of the zonal currents, vertical shear associated with intraseasonal
210 waves, the seasonal varying meridional circulation, and the deep-cycle turbulence contribute to
211 the spatial and temporal variability of equatorial mixing (Heukamp et al. 2022; Moum et al.
212 2022). Using the diapycnal heat flux derived from observations, the seasonal mixed layer heat
213 budget at the equator could be closed to a large extent and the seasonal development of the
214 mixed layer temperatures reasonably well explained (Hummels et al. 2014).

215 An important consequence of upwelling is the increase in biological production that is primarily
216 dependent on nitrate supply (Herbland and Voituriez 1979; Loukos and Memery 1999; Radenac
217 et al. 2020). There is a strong similarity between the seasonal cycles of phytoplankton
218 concentration and SST in the cold tongue area (Fig. 3) (Jouanno et al. 2011b), suggesting that
219 the same physical processes control the downward heat flux out of the mixed layer and the
220 upward supply of nitrate to the euphotic layer. This was confirmed by the analysis of repeated
221 sections of PIRATA and outputs from a coupled physical-biogeochemical model (Radenac et
222 al. 2020). Surface chlorophyll concentrations in the ACT peak in July-August and show a
223 secondary maximum in December-January (Fig. 5a). Radenac et al. (2020) showed that the
224 primary phytoplankton bloom in July-August is due to a strong vertical nitrate input in May-
225 July, and the secondary bloom in December is due to a shorter, moderate input in November-
226 December (Fig. 5b). Analysis of the nitrate balance in the upper ocean suggests that vertical
227 advection controls nitrate input to the equatorial euphotic layer and that vertical diffusion allows
228 nitrate to reach the mixed layer (Figs. 5c, d). However, already noted by Monger et al. (1997),
229 the phytoplankton concentration levels remain high beyond the primary bloom period in July-
230 August, despite the thermocline/nitracline has dropped back to pre-uplift depth in September.
231 Upwelling slightly south of the equator associated with southerly winds or turbulent mixing
232 between EUC and South Equatorial Current were discussed to account for the enhanced nitrate
233 concentration found above the EUC core during that period (Monger et al. 1997; Oudot and
234 Morin 1987).

235



236
237
238
239
240

Fig. 5 Seasonal cycle of vertical profiles of (a) chlorophyll, (b) nitrate, (c) vertical advection, and (d) vertical diffusion in 1.5°S–0.5°N, 20–5°W. The depths of the mixed layer (upper solid line), of the EUC core (dashed line), and of the 20°C isotherm (dotted line) are indicated.

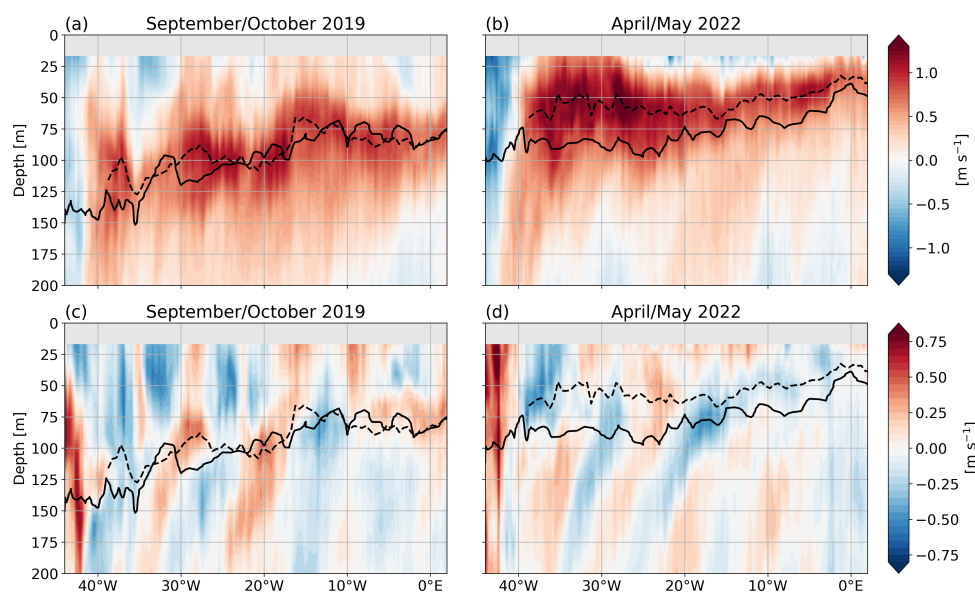
241
242
243
244
245
246

Analysis of the PIRATA sections and model outputs in Radenac et al. (2020) shows that waters transported eastward by the EUC has in general relatively low nitrate concentrations compared to nearby water bodies to the north and south. This is most likely due to the source waters of the EUC that arrive from the oligotrophic layers of the subtropical South Atlantic (Johns et al. 2014; Schott et al. 1998; Tuchen et al. 2022a). The model simulations by Radenac et al. (2020) also revealed that the EUC core does not follow the thermocline depth (as defined as the 20°C



247 isotherm, Figs. 5, 6). While in the eastern equatorial Atlantic, the vertical migration of the
248 thermocline undergoes a semiannual cycle in accordance with the local wind forcing, the EUC
249 core depth has a dominant annual cycle (Brandt et al. 2014). This non-equilibrium response of
250 the equatorial Atlantic to the seasonal wind forcing could be explained by resonant equatorial
251 basin modes composed of eastward and westward propagating equatorial Kelvin and Rossby
252 waves, respectively (Brandt et al. 2016). As the thermocline depth is a good proxy of the
253 nitracline (Fig. 5b), the EUC transports enhanced nitrate and phytoplankton concentrations
254 when the EUC core is close to or deeper than the thermocline or nitracline, which is the case
255 during July-August and to a lesser extent in December (Figs. 5a, b).

256



257

258

259

260

261

262

263

264

265

266

267

268

269

270

271

272

273

274

275

276

277

278

279

Fig. 6 Zonal (a, b) and meridional (c, d) velocity measured along the equator in September-October 2019 (a, c) and in April-May 2022 (b, d). Note, the different colour scales for the zonal and meridional velocities. EUC core depth is marked by dashed lines and the 20°C isotherm (as a proxy of the thermocline and the nitracline) by the solid lines.

Measurements along the equator during two cruises in boreal autumn (Fig. 6a) and boreal spring (Fig. 6b) reveal the basin-wide character of the up- and downward movement of the EUC core relative to the thermocline depths. During boreal autumn, the EUC core closely follows the thermocline, while during boreal spring, it is located clearly above the thermocline. This behaviour can be associated with the resonant equatorial basin mode of the 4th baroclinic mode showing an annual cycle with maximum eastward velocity in the near-surface layer in boreal spring and maximum westward flow in boreal autumn (Brandt et al. 2016). A specific consequence of the relative movement of EUC core and thermocline depth is that the thermocline and thus the nitracline during part of the year vertically migrates into the shear zone above the EUC core. As the upper shear zone of the EUC supports strongly elevated turbulent mixing (Hummels et al. 2013; Hummels et al. 2014; Jouanno et al. 2011b; Moum et al. 2022), enhanced upward nutrient flux occurs during those periods. This was confirmed by the model study of Radenac et al. (2020) showing maxima in the diffusive nitrate flux into the mixed layer in July-August and December (Fig. 5d).

Beside a seasonal cycle, the productivity on the equator shows elevated intraseasonal and shorter-term variability. In particular, tropical instability waves (TIWs) and wind-forced



280 intraseasonal waves play an important role in stimulating locally productivity due to both
281 meridional advection of nitrate and chlorophyll as well as due to events of enhanced vertical
282 advection and mixing (Athie and Marin 2008; Jouanno et al. 2013; Menkes et al. 2002). TIWs
283 are found to be associated with strong mixing events (Moum et al. 2009) or the generation of
284 fronts (Warner et al. 2018) that both can drive upward nutrient supply. Resulting high
285 productivity events could be observed during the boreal autumn cruise that took place shortly
286 after the seasonal maximum of the TIW activity (Sherman et al. 2022).

287

288 **3 Gulf of Guinea upwelling**

289

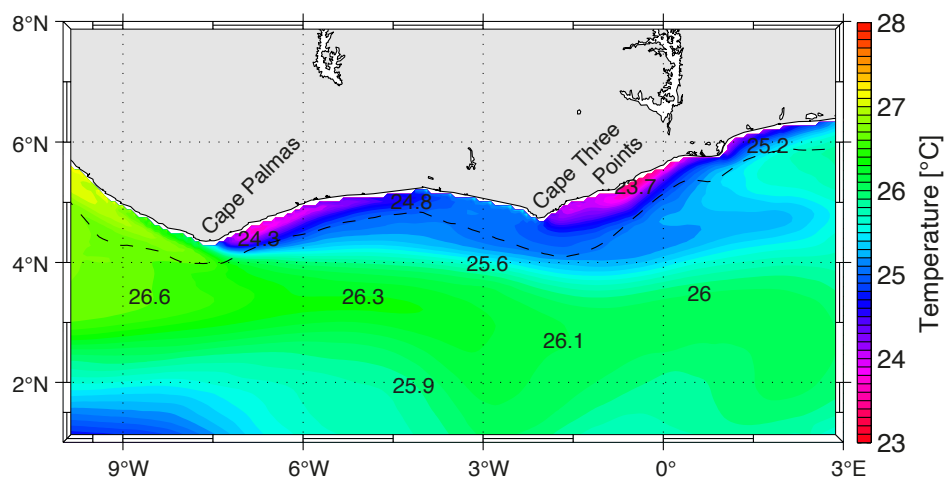
290 In the Gulf of Guinea, coastal upwelling occurs seasonally along the northern coast, between
291 10°W and 5°E, from Côte d'Ivoire to Nigeria (Hardman-Mountford and McGlade 2003). It
292 plays a key role in primary production and local fisheries and is therefore of large socio-
293 economic importance for the bordering countries (Amemou et al. 2020; Koné et al. 2017). SST
294 variability in the GGUS is suggested to modulate the amplitude of the African monsoon and
295 thus has influence on regional climate (Caniaux et al. 2011; Djakouré et al. 2017). The GGUS
296 is constituted of two main upwelling cells, an eastern cell east of Cape Three Points (4°44'N,
297 2°05'W) and a western cell east of Cape Palmas (4°22'N, 7°43'W), that are clearly marked by
298 regions of reduced SST near the coast in satellite data (Wiafe and Nyadjro 2015).

299 Different physical processes have been proposed to explain the presence of the coastal
300 upwelling in the GGUS. In early studies, the coastal upwelling has been related to the
301 strengthening of the geostrophic coastal current. Indeed, the seasonal strengthening in the
302 eastward-flowing Guinea Current contributes to enhance the meridional tilt of the thermocline,
303 thereby bringing cooler subsurface waters near the coast closer to the surface (Bakun 1978;
304 Colin et al. 1993; Ingham 1970). The link between SST and wind stress curl in the GGUS was
305 first suggested by Katz and Garzoli (1982) and Garzoli and Katz (1983). By using a model of
306 the tropical Atlantic, Philander and Pacanowski (1986) showed the influence of both wind
307 components and the wind stress curl on the upwelling in the GGUS. Additionally, Marchal and
308 Picaut (1977) analysed isotherm displacements between Ghana and Côte d'Ivoire and suggested
309 that vertical pumping by cyclonic eddies generated downstream of the capes could explain
310 upwelling of cool waters. However, modelling results by Djakouré et al. (2014) did not confirm
311 that the cyclonic eddies generated downstream of the capes contribute to the upwelling. Instead,
312 Djakouré et al. (2014) and Djakouré et al. (2017) suggest that the upwelling downstream of
313 Cape Palmas is associated with the nonlinear dynamics of the Guinea Current and its
314 detachment from the coast. It is worth noting that the thermocline depth, the strength of the
315 coastal current, and thus the upwelling, are all under the seasonal remote influence of the
316 equatorial ocean through the propagation of equatorial Kelvin and CTWs (Adamec and O'Brien
317 1978; Clarke 1979; Moore et al. 1978; Picaut 1983; Servain et al. 1982). Such remote influence
318 is also indicated by the seasonal cycle of the sea level anomaly along the equatorial and coastal
319 waveguides (Fig. 3b) and was found for intraseasonal wave propagation as well (Imbol
320 Koungue and Brandt 2021; Polo et al. 2008).

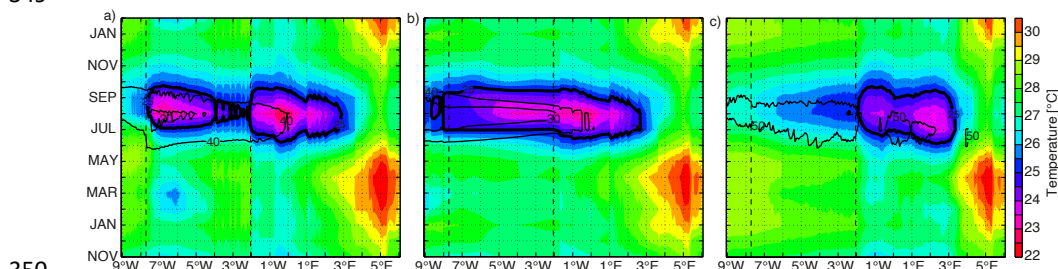
321 By using a model of the tropical Atlantic with an embedded high-resolution nest for the Gulf
322 of Guinea, Djakouré et al. (2014) and Djakouré et al. (2017) performed sensitivity experiments
323 to identify the dominant processes driving the seasonal upwelling in GGUS. The sensitivity
324 includes experiments with a changed coastline without the capes (Djakouré et al. 2014) and
325 with the nonlinear terms responsible for the advection of momentum removed (Djakouré et al.
326 2017). The spatial distribution of the mean SST for the major upwelling season (July-
327 September) is shown for their reference simulation in Fig. 7. A comparison of the sensitivity
328 experiments with the reference simulations (Fig. 8) shows that the sea surface during boreal
329 summer is still colder than the 25°C (chosen as a threshold for the presence of coastal upwelling
330 (Bakun 1978)), when the capes are removed (Fig. 8b). The western upwelling cell disappears



331 only when the nonlinear terms are removed and the Guinea Current is trapped at the coast (Fig.
 332 8c).
 333 The thermocline depth, superimposed on the SST in Fig. 8, is in each of these configurations
 334 closest to the surface during the upwelling season. During this period, in the simulation without
 335 capes, the thermocline has a structure almost identical to that of the realistic configuration.
 336 However, the thermocline depth is always larger than 20 m in the simulation without capes and
 337 thus deeper than in the reference simulation. In the simulation without nonlinear terms, while
 338 generally deeper than in the reference simulation, the thermocline is closer to the surface in the
 339 western upwelling cell than in the eastern upwelling cell (west and east of Cape Three Points,
 340 respectively). The sensitive experiments demonstrated that advection of momentum is the main
 341 contributor to the vertical pumping of the western upwelling cell while the cooling of the eastern
 342 upwelling cell is mainly associated with the wind-induced coastal divergence (Djakouré et al.
 343 2017).
 344



345
 346 **Fig. 7** Mean SST (°C) for the major cold season (July - September) for the reference experiment by Djakouré et
 347 al. (2017). The dashed line represents the 1000 m isobath.
 348
 349

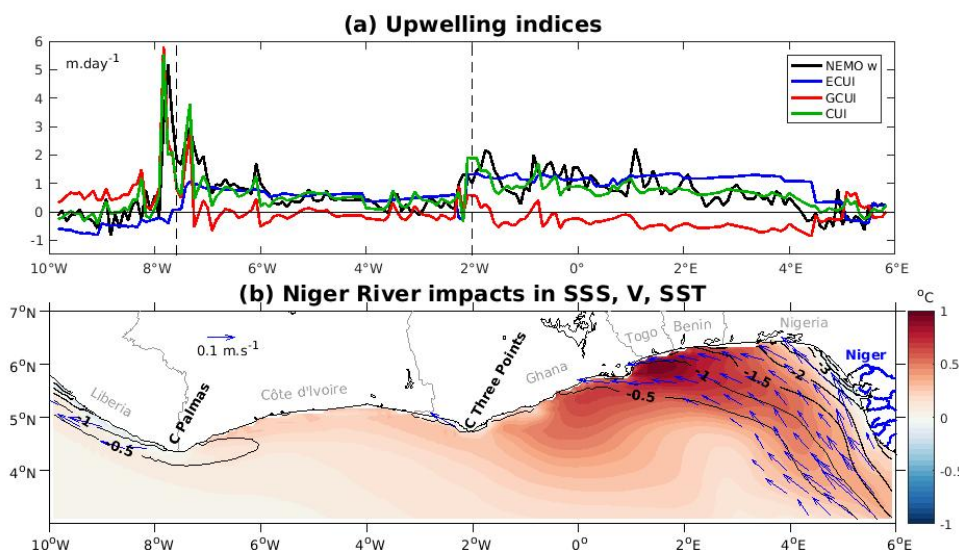


350
 351 **Fig. 8** Hovmöller diagrams of SST (°C) along the coast of the GGUS from 9°W to 6°E of (a) the reference
 352 experiment, the idealized experiments (b) without capes and (c) without inertial terms. The thermocline depth
 353 (20°C isotherm) is superimposed (thin contour lines, unit is m). The vertical dashed black lines represent the
 354 longitude of Cape Palmas and Cape Three Points, see Fig. 7. The time axis in months extends from November to
 355 February of the following year. The 25°C isotherm is additionally marked to highlight the coastal upwelling (thick
 356 contour lines).
 357

358 In the eastern part of the GGUS that is dominantly wind-driven, coastal cooling weakens toward
 359 the east while approaching the Niger River mouth (Fig. 9). Earlier studies have shown that
 360 onshore geostrophic flow can compensate wind-driven offshore transport, thus reducing



361 upwelling in some regions (Marchesiello and Estrade 2010; Rossi et al. 2013). Using a realistic
362 regional model configuration, dynamical Ekman and geostrophic coastal upwelling indices
363 were compared to coastal vertical velocities along the northern Gulf of Guinea coast, during
364 the boreal summer season (Alory et al. 2021). Indeed, the upwelling indices were able to explain
365 a large part of vertical velocity variations all along the coast. They also showed that wind-forced
366 coastal upwelling is reduced by about 50% due to onshore geostrophic flow east of 1°E (Fig.
367 9a). Note that the Ekman index shown in Fig. 9a only takes into account the Ekman transport,
368 as Ekman pumping has little influence in this region (Wiafe and Nyadjro 2015). The onshore
369 geostrophic flow is associated with a sea level slope increasing toward the east. It is driven by
370 density differences along the coast, from relatively cool and salty waters in the upwelling core
371 east of Cape Three Points (Fig. 7) to warm and fresh waters in the Niger River plume and
372 largely compensates offshore Ekman transport and therefore reduces upwelling (Fig. 9a).
373 The comparison of a reference simulation with a simulation in which river run-off is removed,
374 revealed that the Niger River discharge contributes to induce an onshore geostrophic surface
375 flow, but additionally causes a thinning of the mixed layer. Overall, there is no net effect of the
376 river discharge on the near-surface geostrophic transport from which the geostrophic upwelling
377 index is derived. Nevertheless, the Niger River discharge induces a coastal warming reaching
378 1°C near 2°E (Fig. 9b), which is found to be the result of a weakening of turbulent mixing by
379 the enhanced salt stratification (Alory et al. 2021). The summer upwelling season corresponds
380 both to a maximum thinning of the mixed layer and maximum surface chlorophyll concentration
381 along the coast (Toualy et al. 2022). Riverine nutrient inputs may be more or less compensated
382 by a reduced upward nutrient flux due to discharge-driven increased stratification as there is no
383 strong chlorophyll signal in the plume region (Fig. 1).
384



385
386
387 **Fig. 9** (a) Climatological mean (2010-2017) boreal summer (July - September) coastal upwelling index (CUI,
388 defined as the sum of Ekman (ECUI, blue line) and Geostrophic (GCUI, red lines) coastal upwelling
389 indices, compared with coastal vertical velocity at the base of the mixed layer in the reference NEMO simulation
390 (black line). Correlation between the CUI and vertical velocities is 0.72. Vertical dashed lines indicate the location
391 of Cape Palmas and Cape Three Points. (b) River effects on boreal summer sea surface salinity (contour lines),
392 surface geostrophic current (arrows) and sea surface temperature (colour shadings), from a difference between the
393 NEMO reference and a runoff-free simulation.
394



395 **4 Tropical Angolan upwelling**

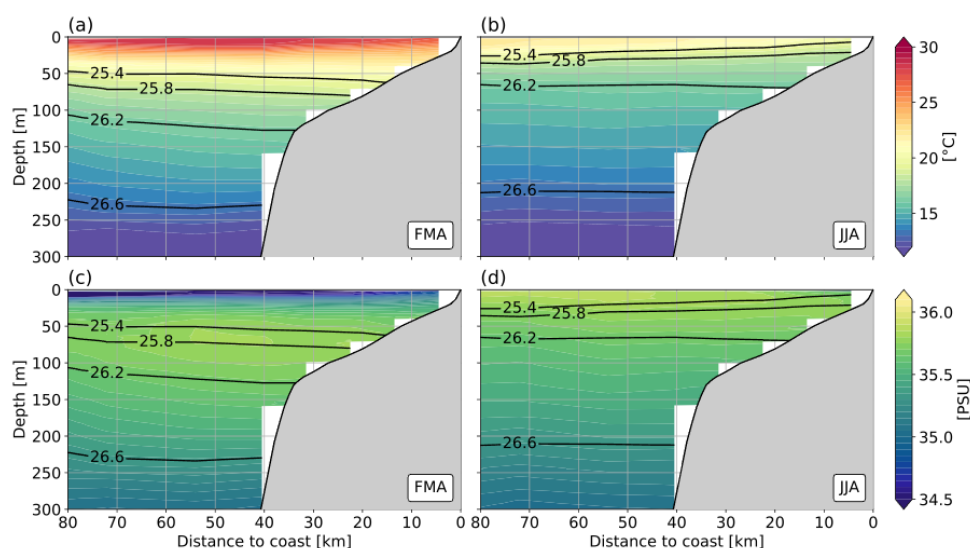
396

397 The Angolan waters host a highly productive ecosystem: the tAUS. Located in the southern
398 hemisphere between the Congo River mouth at 6°S and the Angola-Benguela frontal zone at
399 15°S, the tAUS is of great socio-economic importance for local communities. Fishing supplies
400 about 25% of the total animal protein intake of the Angolan population and is critical for
401 economic security (FAO 2022; Hutchings et al. 2009; Sowman and Cardoso 2010). The
402 productivity in the tAUS undergoes a distinct seasonal cycle (Fig. 4). In the tAUS during austral
403 winter, maximum productivity is observed at the same time as the lowest SST and the strongest
404 cross-shore temperature gradient are present (Awo et al. 2022; Körner et al. 2022; Tchupalanga
405 et al. 2018). In contrast to other eastern boundary upwelling systems, the seasonality of the
406 productivity in the tAUS cannot be explained by local wind forcing (Ostrowski et al. 2009).
407 Prevailing southerly winds in the tAUS are generally weak throughout the year (Fig. 4a).
408 Neither the seasonal cycle of alongshore wind stress nor of the wind stress curl are in phase
409 with the seasonal cycle in productivity suggesting that other mechanisms drive the productivity
410 seasonality in the tAUS (Körner et al. 2022).

411 One of the key dynamics modulating the tAUS on different time scales is the passage of CTWs
412 (Awo et al. 2022; Bachèlery et al. 2016b; Illig et al. 2018b; Kopte et al. 2018; Kopte et al. 2017;
413 Körner et al. 2022; Tchupalanga et al. 2018). CTWs that propagate poleward along the eastern
414 boundary are forced remotely by wind fluctuations along the equator or locally by winds at the
415 eastern boundary. Sea level satellite observations reveal the seasonal passage of four remotely
416 forced CTWs throughout the year (Fig. 4b) (Rouault 2012; Tchupalanga et al. 2018). A
417 downwelling CTW arrives at the Angolan coast in March followed by an upwelling CTW in
418 June/July. A secondary downwelling CTW propagates along the Angolan coast in October
419 followed by a secondary upwelling CTW in December/January. The main component of the
420 eastern boundary circulation in the tAUS is the poleward Angola Current (Kopte et al. 2017;
421 Siegfried et al. 2019). Its variability is linked to equatorial ocean dynamics via the propagations
422 of CTWs at different time scales (Imbol Koungue and Brandt 2021; Kopte et al. 2018; Kopte
423 et al. 2017). On seasonal time scales the southward velocities of the Angola Current peak in
424 October with a secondary maximum in February (Kopte et al. 2017).

425 The hydrographic conditions in the tAUS undergo distinct seasonal changes (Fig. 10).
426 Conductivity, temperature, depth (CTD) data from fifteen years of biannual research cruises of
427 the Nansen program (Tchupalanga et al. 2018) illustrate the seasonal differences between the
428 primary downwelling phase in austral summer and the primary upwelling phase in austral
429 winter (Fig. 10). In austral summer (February-April) the cross-shelf section derived from data
430 averaged between 10°S and 12°S shows warm surface waters and a subsurface salinity
431 maximum. The subsurface salinity maximum is absent in austral winter (June-August). The
432 isopycnals show evidence of down- and upwelling as they bend downward towards the shore
433 in austral summer and upward in austral winter. Furthermore, the isopycnals undergo a vertical
434 displacement between the seasons (the 26.2 kg m⁻³ isopycnal moves vertically by about 50 m).
435 The vertical displacement of the permanent thermocline can be attributed to the passage of
436 CTWs. The seasonal passage of four CTWs induces a semiannual cycle in the vertical isopycnal
437 movements (Kopte et al. 2017; Rouault 2012).

438



439
440 **Fig. 10** Hydrographic conditions between 10°S and 12°S during main downwelling phase, February-April (a,c)
441 and main upwelling phase, June-August (b,d) inferred from the Nansen CTD dataset (Tchpalanga et al. 2018).
442 CTD data is projected on mean topography (GEBCO) between 10°S and 12°S. Panels a and b show the temperature
443 field, panels c and d the salinity field. Black contour lines mark potential density.
444

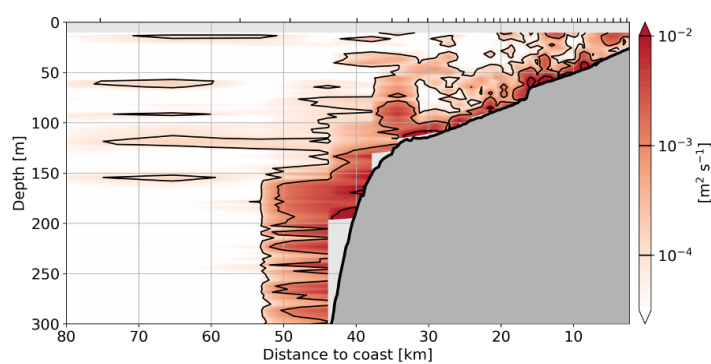
445 To understand the changes in SST in the tAUS, one has to account for other processes than the
446 passage of CTWs. The SST which shows an annual cycle is dominantly driven by the surface
447 heat fluxes. The advection of warm water by the Angola Current plays only a minor role
448 (Körner et al. 2022). In the tAUS, lower SST are found directly along the coast compared to
449 further offshore (Fig. 2). The resulting negative cross-shore SST gradient has a semiannual
450 cycle and is strongest between April and September, with a secondary maximum in
451 December/January. The cross-shore SST gradient can neither be explained by surface heat
452 fluxes which act to dampen the spatial SST differences nor by the weak horizontal heat
453 advection. Ocean turbulence data revealed that turbulent mixing across the base of the mixed
454 layer is strongest in shallow waters and capable of setting up the negative cross-shore SST
455 gradient. The semiannual cycle of the gradient can be explained by turbulent mixing acting
456 upon seasonally different stratifications (Körner et al. 2022) as discussed below.

457 In contrast to SST, sea surface salinity (SSS) in the tAUS undergoes a semiannual cycle. Fresher
458 water is found in the northern part of the tAUS in October/November and in February/March
459 (Fig. 10) (Awo et al. 2022; Kopte et al. 2017; Lübbecke et al. 2019). An important source of
460 freshwater in the tAUS is the Congo River discharge at 6°S, with a maximum discharge into
461 the ocean in early December (Martins and Stammer 2022). The observed freshwater in the
462 tAUS is controlled by meridional advection via the Angola Current and peaks in phase with the
463 strengthening of the Angola Current (Awo et al. 2022). Indeed, the Angola Current displaces
464 the freshwater from the Congo River plume toward the tAUS, leading to elevated stratification
465 with low-salinity water at the surface above a subsurface salinity maximum. This strong
466 stratification favours the subsurface advection of high salinity water counteracting surface
467 freshening via vertical salt advection and mixing at the base of the mixed layer (Awo et al.
468 2022).

469 Turbulent mixing is an important mechanism in the tAUS for the near-coastal cooling, upward
470 salt flux, and upward nutrient supply (Awo et al. 2022; Körner et al. 2022; Ostrowski et al.
471 2009). Ocean turbulence data from six research cruises is used to analyse the distribution of
472 vertical eddy diffusivity at a cross-shelf section at 11°S (Fig. 11). The vertical eddy diffusivity
473 is elevated near the bottom at the continental slope and shelf. Additionally, waters shallower



474 than 75 m show enhanced diffusivities over nearly the whole water column. This finding
475 suggests a dependence of mixing on bathymetry in the tAUS with stronger mixing occurring in
476 shallow waters, similarly to other upwelling systems (Perlin et al. 2005; Schafstall et al. 2010).
477



478
479 **Fig. 11** Vertical eddy diffusivity calculated from microstructure observation as a function of depth and distance to
480 coast. Measurements are taken at a section at about 11°S. Eddy diffusivity is calculated for each profile
481 individually before profiles are binned together in groups of 20 profiles.
482

483 The elevated mixing rates in shallow waters of the tAUS can be explained by the interaction
484 between onshore propagating internal waves and topography. The main energy source of the
485 internal wave field is assumed to be internal tides, which are generated by the interaction of the
486 barotropic tide and the continental slope (Hall et al. 2013; Lamb 2014). By applying a numerical
487 model, Zeng et al. (2021) found that in the tAUS a substantial part of the tidally generated
488 internal wave energy propagates onshore and dissipates in shallow waters. Resulting enhanced
489 near-shore mixing agrees well with observations. The seasonality of the spatially-averaged
490 generation, onshore flux, and dissipation of internal tide energy is weak. This means that
491 throughout the year, roughly the same amount of energy is available for mixing in shallow
492 waters. However, the energy available for mixing acts on seasonally different background
493 stratifications leading to different effects of mixing on temperature (Körner et al. 2022; Zeng
494 et al. 2021). Associated with the passage of CTWs as well as with changes in surface heat fluxes
495 and SSS, the stratification in the tAUS undergoes a semiannual cycle (Kopte et al. 2017). Zeng
496 et al. (2021) showed how cooling in the near coastal area is stronger during phases of weak
497 stratification.

498 The productivity season in the tAUS is in phase with the propagation of CTWs (Fig. 4). The
499 chlorophyll concentration peaks around one month after the passage of the seasonal upwelling
500 CTW in austral winter. Similarly, a secondary chlorophyll peak is visible after the passage of
501 the secondary upwelling CTW in December/January. However, the exact process of how the
502 passage of the CTWs leads to an increase in primary production remains an open question. The
503 seasonal varying effect of mixing on SSTs shows that a reduction in stratification can lead to
504 more effective cooling near the coast during the upwelling phase (Körner et al. 2022; Zeng et
505 al. 2021). The upward nutrient supply additionally depends on the change in the background
506 distribution of nutrients. Higher upward nutrient fluxes could be achieved by increasing the
507 nutrient gradient during phases of upwelling CTW in areas of high mixing. Such changes in
508 background conditions associated with the onshore advection of nutrients during the passage
509 of CTWs might be able to ultimately explain the seasonal productivity signals in the tAUS.
510

511 **5 Relation between upwelling seasonality and longer-term variability**

512

513 The seasonal upwelling has important consequences on the expression of the interannual
514 variability at the sea surface of the tropical Atlantic. It is the area and season most impacted by



515 the upwelling that show marked interannual variability, whether in terms of SST (Keenlyside
516 and Latif 2007) or phytoplankton concentration (Chenillat et al. 2021).
517 The dominant climate mode in the tropical Atlantic is the Atlantic Niño (Hisard 1980; Lübbecke
518 et al. 2018; Ruiz-Barradas et al. 2000). It is most pronounced in the equatorial cold tongue east
519 of 23°W and peaks during boreal summer. Anomalous warm or cold events are thus associated
520 with anomalous deep or shallow thermocline and correspondingly with reduced or enhanced
521 upwelling, respectively. The Atlantic Niño is associated with SSS variability as well (Awo et
522 al. 2018) suggesting an additionally forcing of the equatorial and eastern boundary upwelling
523 in the eastern tropical Atlantic by the impact of precipitation and river discharge on near-surface
524 stratification. Besides the interannual variability, decadal variability can impact the equatorial
525 upwelling. Such variability might be associated with a changing strength of the STCs forced by
526 off-equatorial easterlies (Rabe et al. 2008; Tuchen et al. 2020). Similarly, Brandt et al. (2021)
527 found an intensification of the EUC for the period 2008-2018 that was linked to enhanced trade
528 winds in the tropical North Atlantic likely associated with the Atlantic multidecadal variability
529 (Knight et al. 2006). Other mechanisms that are suggested to impact the strength of equatorial
530 cooling on decadal time scales include the decadal variability of TIWs. A decadal strengthening
531 of TIWs was found to be associated with enhanced warming of the equatorial cold tongue by
532 lateral eddy fluxes (Tuchen et al. 2022b). Coupled climate simulations also suggest the
533 importance of surface heat fluxes in driving interannual to decadal cold tongue SST variability
534 (Nnamchi et al. 2015). As discussed by Jouanno et al. (2017), such heat flux forcing is likely
535 overemphasized due to large upper ocean temperature biases commonly found in climate
536 models. Chang et al. (2008) analysed the impact of a changing Atlantic meridional overturning
537 circulation (AMOC) on the tropical Atlantic using simulations with a climate model. These
538 simulations showed that a weakened AMOC results in a warmer equatorial Atlantic with
539 reduced seasonal cycle and interannual variability. Similarly, a weakening of interannual
540 variability is projected under a global warming scenario (Crespo et al. 2022). However, the
541 impact of global warming or reduced AMOC on seasonal or interannual variability of
542 productivity is highly uncertain as even the impact on upper ocean stratification is not coherent
543 between different models and datasets, which is partly due to the fact that first decadal trends
544 in stratification or productivity are just emerging (Hammond et al. 2020; Roch et al. 2021;
545 Sallee et al. 2021).
546 In the GGUS, interannual variability is generally stronger in regions of strong seasonal
547 variability as has been documented from satellite and in situ data (Sohou et al. 2020; Wiafe and
548 Nyadjro 2015). Potential drivers of interannual variability are similar to drivers of seasonal
549 changes. They include changes in the wind forcing and turbulent mixing, and remote forcing
550 associated with the Atlantic Niño (Jouanno et al. 2017; Wade et al. 2011). Processes involved
551 in the 2012 cold anomalies in the GGUS, the coldest event observed over the last 30 years, have
552 been investigated through a model heat budget (Da-Allada et al. 2021). Results revealed that
553 the surface cooling at Cape Palmas was driven by changes in zonal advection and increased
554 turbulent mixing due a strengthening of the Guinea Current and associated vertical shear, while
555 east at Cape Three Point, it was driven by a strengthening of the zonal wind stress that increased
556 the offshore Ekman transport.
557 Benguela Niños and Niñas are the dominant mode of interannual climate variability in the tAUS
558 (Shannon et al. 1986). Contrary to the variability in the EAUS and GGUS, seasonally
559 interannual variability does not reach its maximum during the main upwelling season, but
560 during the main downwelling season from March to May (Lübbecke et al. 2019). During a
561 Benguela Niño or Niña, SST can be up to 2°C higher or lower than the climatology in the tAUS
562 (Imbol Koungue et al. 2021; Imbol Koungue et al. 2019; Rouault et al. 2007; Rouault et al.
563 2018). These extreme events have drastic consequences for the marine ecosystem (Gammelsrød
564 et al. 1998) through modulations in coastal upwelling intensity, nutrients and oxygen content
565 along the continental shelf (Bachèlery et al. 2016a). It can be assumed that forcing mechanisms



566 of Benguela Niños and Niñas are similar to those of the seasonal upwelling variability. On one
567 hand, winds at the equator can generate equatorial Kelvin waves (Illig et al. 2004) that continue
568 southward along the southwest African coast as CTWs and produce locally thermocline
569 displacements (Bachèlery et al. 2016b; Bachèlery et al. 2020; Imbol Koungue et al. 2017; Polo
570 et al. 2008). On the other hand, fluctuations of local alongshore winds (Richter et al. 2010) and
571 other local processes such as freshwater inputs (Lübbecke et al. 2019) further generate SST
572 anomalies in the tAUS. For the satellite era, Prigent et al. (2020a) showed a weakening of
573 interannual SST variability in the southeastern tropical Atlantic between 2000-2017 relative to
574 1982-1999. However, since 2018, two consecutive extreme coastal warm events have been
575 recorded in the tAUS in 2019/2020 (Imbol Koungue et al. 2021) and in 2021. The recent
576 decades demonstrate a strong warming trend in the tropical Atlantic SST with the largest
577 warming observed in the coastal upwelling regions off southwestern Africa including the tAUS
578 (Tokinaga and Xie 2011). Moreover, using observational data, Roch et al. (2021) discovered a
579 change in upper-ocean stratification from subtropical to tropical conditions associated with a
580 warming and freshening of the mixed layer between 2006 and 2020 in the southeastern tropical
581 Atlantic (10°S-20°S; 5°W-15°E). Such changes in stratification are assumed to particularly
582 impact the mixing-driving nitrate supply in the tAUS.

583

584 **6 Conclusion and outlook**

585

586 Here we have reviewed the physical processes in three major upwelling systems of the inner
587 tropical Atlantic, the EAUS, the GGUS, and the tAUS, that drive the upwelling seasonality.
588 Among them are the processes that locally impact the thermocline depth - often used as a proxy
589 of the nitracline - such as zonal wind along the equator, alongshore wind and wind stress curl
590 in coastal upwelling regions or the detachment of the boundary current. Remote processes
591 associated with the propagation of equatorial Kelvin and CTWs affect the thermocline depth in
592 the different upwelling regions on intraseasonal, seasonal and interannual timescales as well.
593 The processes affecting the thermocline depth can be summarized under locally and remotely
594 driven vertical advection which is able to transfer colder and nutrient-rich waters upward to the
595 surface during active upwelling. Additionally, diffusive fluxes associated with turbulent mixing
596 at the base of the mixed layer and within the thermocline transport heat downward and nutrients
597 upward.

598 The EAUS can be characterized as a wind-driven upwelling system forced by different wind
599 components at the equator and off the equator. Wind changes generate upwelling and
600 downwelling equatorial waves propagating along the equator and adjust the equatorial
601 thermocline to reach an equilibrium with the wind forcing. The zonal velocity field instead is
602 dominated by the equatorial basin resonance of the 2nd and 4th baroclinic modes resulting in an
603 EUC that vertically migrate largely independent of the thermocline (Brandt et al. 2016). During
604 periods, when the thermocline depth is shallower than the EUC core, turbulent mixing in the
605 shear zone above the core of the EUC is essential for the downward heat flux and upward nitrate
606 flux out and into the mixed layer, respectively (Hummels et al. 2014; Jouanno et al. 2011b). In
607 the GGUS different processes define the two upwelling centres, east of Cape Palmas and east
608 of Cape Three Points. East of Cape Palmas, the nonlinear detachment of Guinea Current from
609 the coast plays the most important role, while east of Cape Three Points, upwelling is mainly
610 associated with the wind-induced coastal divergence (Djakouré et al. 2017). The upwelling in
611 the tAUS, which is characterized by weak winds, is dominantly driven by a combination of
612 remotely forced CTWs and locally induced turbulent mixing (Körner et al. 2022; Rouault 2012;
613 Tchicalanga et al. 2018).

614 Climate warming and change might impact the upwelling in the different regions and its
615 seasonality (amplitude and phase) differently. Most obvious are probably future changes in the
616 wind field, e.g., a strengthening of the winds in a warming world or poleward shifts of the main



617 wind systems (Yang et al. 2020). Changes in the stratification and mixed layer depths are highly
618 uncertain with recent studies suggesting an increase of the stratification at the base of the mixed
619 layer together with a mixed layer deepening likely due to enhanced wind-driven upper-ocean
620 turbulent mixing (Sallee et al. 2021). However, other processes such as lateral mixing,
621 responsible for reducing nitrate concentrations in upwelling regions, or surface heat fluxes,
622 might contribute as well. Recently, the multidecadal increase in the strength of TIWs and
623 associated equatorward eddy heat flux was suggested to warm the EAUS (Tuchen et al. 2022b).
624 Such eddy fluxes generally oppose the Ekman transport in upwelling systems. Air-sea heat and
625 buoyancy fluxes were identified to modulate such compensation in idealized model simulations
626 (Thomsen et al. 2021), suggesting that in a warming climate also changes in heat and freshwater
627 fluxes have the potential to impact the upwelling strength via its impact on lateral eddy fluxes.
628 The identification of climate changes in upwelling systems is a major goal that requires the
629 maintenance and further development of the tropical Atlantic observing system (Foltz et al.
630 2019). In particular, coastal upwelling regions show a sparse data coverage and the
631 strengthening of the near-coastal observing system has a high priority. This requires a close
632 cooperation with the coastal communities to jointly develop the research agenda according to
633 collective interests and needs. Main questions regard the often-competing role of changes in
634 wind forcing and stratification and the role of changing eddy fluxes and buoyancy forcing.
635 What will be the consequences of changing upwelling amplitude and/or timing for
636 biogeochemistry and biology? Overall, future upwelling studies require a close cooperation
637 between different research disciplines focussing on the interaction between the physical,
638 biogeochemical and biological systems and allowing an improved assessment of ecosystem
639 management and fisheries.

640

641 **Data availability**

642

643 Publicly available datasets were used for this study. Chlorophyll data are from the Copernicus-
644 GlobColour dataset (<https://doi.org/10.48670/moi-00021>). The sea level anomaly data were
645 accessed via the Copernicus Server (<https://doi.org/10.48670/moi-00148>). Microwave OI SST
646 and wind data from ASCAT and QSCAT are available under <https://www.remss.com>. Also
647 used are surface wind stress from ERA5 (<https://cds.climate.copernicus.eu/>). Hydrographic
648 sections in Angolan waters have been produced using the Nansen CTD Dataset
649 (<https://doi.pangaea.de/10.1594/PANGAEA.887163>).

650

651 **Author contribution**

652

653 PB outlined and wrote the manuscript. MK, RI, JJ, SD, GA produced the figures. All co-authors
654 contributed to and reviewed the manuscript.

655

656 **Appendix A**

657

658 List of abbreviations.

659	AMOC	Atlantic meridional overturning circulation
660	ACT	Atlantic cold tongue
661	CTD	conductivity, temperature, depth
662	CTW	coastally trapped wave
663	EAUS	equatorial Atlantic upwelling system
664	EUC	Equatorial Undercurrent
665	FAO	Food and Agriculture Organization
666	GGUS	Gulf of Guinea upwelling system
667	tAUS	tropical Angolan upwelling system



668 TIWs tropical instability waves
669 SSS sea surface salinity
670 SST sea surface temperature
671 STC subtropical cells

672

673 **Acknowledgements**

674

675 The study was funded by EU H2020 under grant agreement 817578 TRIATLAS project. It was
676 further supported by the German Federal Ministry of Education and Research as part of the
677 BANINO (03F0795A) project.

678



679

References

680

681 Adamec D, Obrien JJ (1978) Seasonal upwelling in Gulf of Guinea due to remote forcing.
682 *Journal of Physical Oceanography* 8:1050-1060. [https://doi.org/10.1175/1520-0485\(1978\)008<1050:Tsuitg>2.0.Co;2](https://doi.org/10.1175/1520-0485(1978)008<1050:Tsuitg>2.0.Co;2)

684 Alory G, Da-Allada CY, Djakouré S et al (2021) Coastal Upwelling Limitation by Onshore
685 Geostrophic Flow in the Gulf of Guinea Around the Niger River Plume. *Frontiers in*
686 *Marine Science* 7:607216. <https://doi.org/10.3389/fmars.2020.607216>

687 Amemou H, Koné V, Aman A et al (2020) Assessment of a Lagrangian model using trajectories
688 of oceanographic drifters and fishing devices in the Tropical Atlantic Ocean. *Progress*
689 *in Oceanography* 188:102426. <https://doi.org/10.1016/j.pocean.2020.102426>

690 Athie G, Marin F (2008) Cross-equatorial structure and temporal modulation of intraseasonal
691 variability at the surface of the Tropical Atlantic Ocean. *Journal of Geophysical*
692 *Research-Oceans* 113:C08020. <https://doi.org/10.1029/2007jc004332>

693 Awo FM, Alory G, Da-Allada CY et al (2018) Sea Surface Salinity Signature of the Tropical
694 Atlantic Interannual Climatic Modes. *Journal of Geophysical Research-Oceans*
695 123:7420-7437. <https://doi.org/10.1029/2018jc013837>

696 Awo FM, Rouault M, Ostrowski M et al (2022) Seasonal cycle of sea surface salinity in the
697 Angola Upwelling System. *Journal of Geophysical Research-Oceans*
698 127:e2022JC018518. <https://doi.org/10.1029/2022JC018518>

699 Bachèlery ML, Illig S, Dadou I (2016a) Forcings of nutrient, oxygen, and primary production
700 interannual variability in the southeast Atlantic Ocean. *Geophysical Research Letters*
701 43:8617-8625. <https://doi.org/10.1002/2016gl070288>

702 Bachèlery ML, Illig S, Dadou I (2016b) Interannual variability in the South-East Atlantic Ocean,
703 focusing on the Benguela Upwelling System: Remote versus local forcing. *Journal of*
704 *Geophysical Research-Oceans* 121:284-310. <https://doi.org/10.1002/2015jc011168>

705 Bachèlery ML, Illig S, Rouault M (2020) Interannual coastal trapped waves in the Angola-
706 Benguela upwelling system and Benguela Niño and Niña events. *Journal of Marine*
707 *Systems* 203:103262. <https://doi.org/10.1016/j.jmarsys.2019.103262>

708 Bakun A (1978) Guinea Current Upwelling. *Nature* 271:147-150. <https://doi.org/10.1038/271147a0>

710 Bourlès B, D'Orgeville M, Eldin G et al (2002) On the evolution of the thermocline and
711 subthermocline eastward currents in the Equatorial Atlantic. *Geophysical Research*
712 *Letters* 29:32.1-32.4. <https://doi.org/10.1029/2002gl015098>

713 Brandt P, Caniaux G, Bourlès B et al (2011) Equatorial upper-ocean dynamics and their
714 interaction with the West African monsoon. *Atmospheric Science Letters* 12:24-30.
715 <https://doi.org/10.1002/Asl.287>

716 Brandt P, Claus M, Greatbatch RJ et al (2016) Annual and semiannual cycle of equatorial
717 Atlantic circulation associated with basin-mode resonance. *Journal of Physical*
718 *Oceanography* 46:3011-3029. <https://doi.org/10.1175/Jpo-D-15-0248.1>

719 Brandt P, Funk A, Tantet A et al (2014) The Equatorial Undercurrent in the central Atlantic and
720 its relation to tropical Atlantic variability. *Climate Dynamics* 43:2985-2997. <https://doi.org/10.1007/s00382-014-2061-4>

722 Brandt P, Hahn J, Schmidtko S et al (2021) Atlantic Equatorial Undercurrent intensification
723 counteracts warming-induced deoxygenation. *Nature Geoscience* 14:278-282. <https://doi.org/10.1038/s41561-021-00716-1>

724



- 725 Burls NJ, Reason CJC, Penven P et al (2011) Similarities between the tropical Atlantic seasonal
726 cycle and ENSO: An energetics perspective. *Journal of Geophysical Research-Oceans*
727 116:C11010. <https://doi.org/10.1029/2011jc007164>
- 728 Cai WJ, Wang GJ, Dewitte B et al (2018) Increased variability of eastern Pacific El Niño under
729 greenhouse warming. *Nature* 564:201-206. <https://doi.org/10.1038/s41586-018-0776-9>
- 730
- 731 Caniaux G, Giordani H, Redelsperger JL et al (2011) Coupling between the Atlantic cold tongue
732 and the West African monsoon in boreal spring and summer. *Journal of Geophysical*
733 *Research-Oceans* 116:C04003. <https://doi.org/10.1029/2010jc006570>
- 734 Chang P, Zhang R, Hazeleger W et al (2008) Oceanic link between abrupt changes in the North
735 Atlantic Ocean and the African monsoon. *Nature Geoscience* 1:444-448. <https://doi.org/10.1038/Ngeo218>
- 736
- 737 Chenillat F, Illig S, Jouanno J et al (2021) How do climate modes shape the Chlorophyll-a
738 interannual variability in the tropical Atlantic? *Geophysical Research Letters*
739 48:e2021GL093769. <https://doi.org/10.1029/2021GL093769>
- 740 Clarke AJ (1979) On the generation of the seasonal coastal upwelling in the Gulf of Guinea.
741 *Journal of Geophysical Research-Oceans and Atmospheres* 84:3743-3751. <https://doi.org/10.1029/JC084iC07p03743>
- 742
- 743 Colin C, Gallardo Y, Chuchla R et al (1993) Environnements climatique et océanographique sur
744 le plateau continental de Côte d'Ivoire. In: Le Loeuff P, Marchal E, Amon Kothias JB
745 (eds) *Environnement et ressources aquatiques de Côte d'Ivoire : 1. Le milieu marin*.
746 ORSTOM, Paris, pp 75-110.
- 747 Crespo LR, Prigent A, Keenlyside N et al (2022) Weakening of the Atlantic Niño variability under
748 global warming. *Nature Climate Change* 12:822-827. <https://doi.org/10.1038/s41558-022-01453-y>
- 749
- 750 Da-Allada CY, Agada J, Baloitcha E et al (2021) Causes of the Northern Gulf of Guinea Cold
751 Event in 2012. *Journal of Geophysical Research-Oceans* 126:e2021JC017627. <https://doi.org/10.1029/2021JC017627>
- 752
- 753 Ding H, Keenlyside NS, Latif M (2009) Seasonal cycle in the upper equatorial Atlantic Ocean.
754 *Journal of Geophysical Research-Oceans* 114:C09016. <https://doi.org/10.1029/2009jc005418>
- 755
- 756 Djakouré S, Penven P, Bourlès B et al (2017) Respective roles of the Guinea Current and local
757 winds on the coastal upwelling in the northern Gulf of Guinea. *Journal of Physical*
758 *Oceanography* 47:1367-1387. <https://doi.org/10.1175/Jpo-D-16-0126.1>
- 759 Djakouré S, Penven P, Bourlès B et al (2014) Coastally trapped eddies in the north of the Gulf
760 of Guinea. *Journal of Geophysical Research-Oceans* 119:6805-6819. <https://doi.org/10.1002/2014jc010243>
- 761
- 762 FAO (2022) *Fishery and Aquaculture Country Profiles. Angola. Country Profile Fact Sheets*.
763 Fisheries and Aquaculture Division [online]. Rome.
- 764 Foltz GR, Brandt P, Richter I et al (2019) The Tropical Atlantic Observing System. *Frontiers in*
765 *Marine Science* 6:206. <https://doi.org/10.3389/fmars.2019.00206>
- 766 Fu Y, Brandt P, Tuchen FP et al (2022) Representation of the mean Atlantic subtropical cells in
767 CMIP6 models. *Journal of Geophysical Research-Oceans* 127:e2021JC018191. <https://doi.org/10.1029/2021JC018191>
- 768
- 769 Gammelsrød T, Bartholomae CH, Boyer DC et al (1998) Intrusion of warm surface water along
770 the Angolan-Namibian coast in February-March 1995: The 1995 Benguela Niño. *South*
771 *African Journal of Marine Science-Suid-Afrikaanse Tydskrif Vir Seewetenskap* 19:41-
772 56. <https://doi.org/10.2989/025776198784126719>



- 773 Garzoli SL, Katz EJ (1983) The Forced Annual Reversal of the Atlantic North Equatorial
774 Countercurrent. *Journal of Physical Oceanography* 13:2082-2090. [https://doi.org/](https://doi.org/10.1175/1520-0485(1983)013<2082:Tfarot>2.0.Co;2)
775 10.1175/1520-0485(1983)013<2082:Tfarot>2.0.Co;2
- 776 Giordani H, Caniaux G (2011) Diagnosing vertical motion in the Equatorial Atlantic. *Ocean*
777 *Dynamics* 61:1995-2018. <https://doi.org/10.1007/s10236-011-0467-7>
- 778 Grodsky SA, Carton JA, McClain CR (2008) Variability of upwelling and chlorophyll in the
779 equatorial Atlantic. *Geophysical Research Letters* 35:L03610. [https://doi.org/](https://doi.org/10.1029/2007gl032466)
780 10.1029/2007gl032466
- 781 Hall RA, Huthnance JM, Williams RG (2013) Internal wave reflection on shelf slopes with
782 depth-varying stratification. *Journal of Physical Oceanography* 43:248-258. [https://](https://doi.org/10.1175/Jpo-D-11-0192.1)
783 doi.org/10.1175/Jpo-D-11-0192.1
- 784 Hammond ML, Beaulieu C, Henson SA et al (2020) Regional surface chlorophyll trends and
785 uncertainties in the global ocean. *Scientific Reports* 10:15273. [https://doi.org/](https://doi.org/10.1038/s41598-020-72073-9)
786 10.1038/s41598-020-72073-9
- 787 Hardman-Mountford NJ, McGlade JM (2003) Seasonal and interannual variability of
788 oceanographic processes in the Gulf of Guinea: an investigation using AVHRR sea
789 surface temperature data. *International Journal of Remote Sensing* 24:3247-3268.
790 <https://doi.org/10.1080/0143116021000021297>
- 791 Herbert G, Bourlès B, Penven P et al (2016) New insights on the upper layer circulation north
792 of the Gulf of Guinea. *Journal of Geophysical Research-Oceans* 121:6793-6815.
793 <https://doi.org/10.1002/2016jc011959>
- 794 Herbland A, Voituriez B (1979) Hydrological Structure-Analysis for Estimating the Primary
795 Production in the Tropical Atlantic Ocean. *Journal of Marine Research* 37:87-101.
- 796 Heukamp FO, Brandt P, Dengler M et al (2022) Tropical instability waves and wind-forced
797 cross-equatorial flow in the central Atlantic Ocean. *Geophysical Research Letters*
798 49:e2022GL099325. <https://doi.org/10.1029/2022GL099325>
- 799 Hisard P (1980) El-Niño response of the eastern Tropical Atlantic. *Oceanologica Acta* 3:69-78.
- 800 Hormann V, Brandt P (2009) Upper equatorial Atlantic variability during 2002 and 2005
801 associated with equatorial Kelvin waves. *Journal of Geophysical Research-Oceans*
802 114:C03007. <https://doi.org/10.1029/2008jc005101>
- 803 Hummels R, Dengler M, Bourlès B (2013) Seasonal and regional variability of upper ocean
804 diapycnal heat flux in the Atlantic cold tongue. *Progress in Oceanography* 111:52-74.
805 <https://doi.org/10.1016/j.pocean.2012.11.001>
- 806 Hummels R, Dengler M, Brandt P et al (2014) Diapycnal heat flux and mixed layer heat budget
807 within the Atlantic Cold Tongue. *Climate Dynamics* 43:3179-3199. [https://doi.org/](https://doi.org/10.1007/s00382-014-2339-6)
808 10.1007/s00382-014-2339-6
- 809 Hutchings L, van der Lingén CD, Shannon LJ et al (2009) The Benguela Current: An ecosystem
810 of four components. *Progress in Oceanography* 83:15-32. [https://doi.org/](https://doi.org/10.1016/j.pocean.2009.07.046)
811 10.1016/j.pocean.2009.07.046
- 812 Illig S, Bachèlery ML, Cadier E (2018a) Subseasonal coastal-trapped wave propagations in the
813 southeastern Pacific and Atlantic oceans: 2. Wave characteristics and connection with
814 the equatorial variability. *Journal of Geophysical Research-Oceans* 123:3942-3961.
815 <https://doi.org/10.1029/2017jc013540>
- 816 Illig S, Cadier E, Bachèlery ML et al (2018b) Subseasonal coastal-trapped wave propagations in
817 the southeastern Pacific and Atlantic oceans: 1. A new approach to estimate wave
818 amplitude. *Journal of Geophysical Research-Oceans* 123:3915-3941. [https://doi.org/](https://doi.org/10.1029/2017jc013539)
819 10.1029/2017jc013539



- 820 Illig S, Dewitte B, Ayoub N et al (2004) Interannual long equatorial waves in the tropical
821 Atlantic from a high-resolution ocean general circulation model experiment in 1981-
822 2000. *Journal of Geophysical Research-Oceans* 109:C02022. [https://doi.org/](https://doi.org/10.1029/2003jc001771)
823 [10.1029/2003jc001771](https://doi.org/10.1029/2003jc001771)
- 824 Imbol Kougue RA, Brandt P (2021) Impact of intraseasonal waves on Angolan warm and cold
825 events. *Journal of Geophysical Research-Oceans* 126:e2020JC017088. [https://doi.org/](https://doi.org/10.1029/2020JC017088)
826 [10.1029/2020JC017088](https://doi.org/10.1029/2020JC017088)
- 827 Imbol Kougue RA, Brandt P, Lübbecke JF et al (2021) The 2019 Benguela Niño. *Frontiers in*
828 *Marine Science* 8:800103. <https://doi.org/10.3389/fmars.2021.800103>
- 829 Imbol Kougue RA, Illig S, Rouault M (2017) Role of interannual Kelvin wave propagations in
830 the equatorial Atlantic on the Angola Benguela Current system. *Journal of Geophysical*
831 *Research-Oceans* 122:4685-4703. <https://doi.org/10.1002/2016jc012463>
- 832 Imbol Kougue RA, Rouault M, Illig S et al (2019) Benguela Niños and Benguela Niñas in Forced
833 Ocean Simulation From 1958 to 2015. *Journal of Geophysical Research-Oceans*
834 124:5923-5951. <https://doi.org/10.1029/2019jc015013>
- 835 Ingham MC (1970) Coastal upwelling in northwestern Gulf of Guinea. *Bulletin of Marine*
836 *Science* 20:1-34.
- 837 Johns WE, Brandt P, Bourlès B et al (2014) Zonal structure and seasonal variability of the
838 Atlantic Equatorial Undercurrent. *Climate Dynamics* 43:3047-3069. [https://doi.org/](https://doi.org/10.1007/s00382-014-2136-2)
839 [10.1007/s00382-014-2136-2](https://doi.org/10.1007/s00382-014-2136-2)
- 840 Jouanno J, Hernandez O, Sanchez-Gomez E (2017) Equatorial Atlantic interannual variability
841 and its relation to dynamic and thermodynamic processes. *Earth System Dynamics*
842 8:1061-1069. <https://doi.org/10.5194/esd-8-1061-2017>
- 843 Jouanno J, Marin F, du Penhoat Y et al (2013) Intraseasonal modulation of the surface cooling
844 in the Gulf of Guinea. *Journal of Physical Oceanography* 43:382-401. [https://doi.org/](https://doi.org/10.1175/Jpo-D-12-053.1)
845 [10.1175/Jpo-D-12-053.1](https://doi.org/10.1175/Jpo-D-12-053.1)
- 846 Jouanno J, Marin F, du Penhoat Y et al (2011a) Seasonal modes of surface cooling in the Gulf
847 of Guinea. *Journal of Physical Oceanography* 41:1408-1416. [https://doi.org/](https://doi.org/10.1175/Jpo-D-11-031.1)
848 [10.1175/Jpo-D-11-031.1](https://doi.org/10.1175/Jpo-D-11-031.1)
- 849 Jouanno J, Marin F, du Penhoat Y et al (2011b) Seasonal heat balance in the upper 100 m of
850 the equatorial Atlantic Ocean. *Journal of Geophysical Research-Oceans* 116:C09003.
851 <https://doi.org/10.1029/2010jc006912>
- 852 Katz EJ, Garzoli S (1982) Response of the western Equatorial Atlantic Ocean to an annual wind
853 cycle. *Journal of Marine Research* 40:307-327.
- 854 Keenlyside NS, Latif M (2007) Understanding equatorial Atlantic interannual variability.
855 *Journal of Climate* 20:131-142. <https://doi.org/10.1175/Jcli3992.1>
- 856 Kiko R, Biastoch A, Brandt P et al (2017) Biological and physical influences on marine snowfall
857 at the equator. *Nature Geoscience* 10:852-858. <https://doi.org/10.1038/Ngeo3042>
- 858 Knight JR, Folland CK, Scaife AA (2006) Climate impacts of the Atlantic Multidecadal
859 Oscillation. *Geophysical Research Letters* 33:L17706. [https://doi.org/](https://doi.org/10.1029/2006gl026242)
860 [10.1029/2006gl026242](https://doi.org/10.1029/2006gl026242)
- 861 Kolodziejczyk N, Marin F, Bourlès B et al (2014) Seasonal variability of the equatorial
862 undercurrent termination and associated salinity maximum in the Gulf of Guinea.
863 *Climate Dynamics* 43:3025-3046. <https://doi.org/10.1007/s00382-014-2107-7>
- 864 Koné V, Lett C, Penven P et al (2017) A biophysical model of *S. aurita* early life history in the
865 northern Gulf of Guinea. *Progress in Oceanography* 151:83-96. [https://doi.org/](https://doi.org/10.1016/j.pcean.2016.10.008)
866 [10.1016/j.pcean.2016.10.008](https://doi.org/10.1016/j.pcean.2016.10.008)



- 867 Kopte R, Brandt P, Claus M et al (2018) Role of equatorial basin-mode resonance for the
868 seasonal variability of the Angola Current at 11°S. *Journal of Physical Oceanography*
869 48:261-281. <https://doi.org/10.1175/Jpo-D-17-0111.1>
- 870 Kopte R, Brandt P, Dengler M et al (2017) The Angola Current: Flow and hydrographic
871 characteristics as observed at 11°S. *Journal of Geophysical Research-Oceans* 122:1177-
872 1189. <https://doi.org/10.1002/2016jc012374>
- 873 Körner M, Brandt P, Dengler M (2022) Seasonal cycle of sea surface temperature in the
874 tropical Angolan upwelling system. *EGUsphere* 1-33. <https://doi.org/10.5194/egusphere-2022-973>
- 876 Lamb KG (2014) Internal wave breaking and dissipation mechanisms on the continental
877 slope/shelf. *Annual Review of Fluid Mechanics*, Vol 46 46:231-254. <https://doi.org/10.1146/annurev-fluid-011212-140701>
- 879 Longhurst A (1993) Seasonal cooling and blooming in tropical oceans. *Deep-Sea Research Part*
880 *I-Oceanographic Research Papers* 40:2145-2165. [https://doi.org/10.1016/0967-0637\(93\)90095-K](https://doi.org/10.1016/0967-0637(93)90095-K)
- 882 Loukos H, Memery L (1999) Simulation of the nitrate seasonal cycle in the equatorial Atlantic
883 Ocean during 1983 and 1984. *Journal of Geophysical Research-Oceans* 104:15549-
884 15573. <https://doi.org/10.1029/1999jc900084>
- 885 Lübbecke JF, Brandt P, Dengler M et al (2019) Causes and evolution of the southeastern
886 tropical Atlantic warm event in early 2016. *Climate Dynamics* 53:261-274. <https://doi.org/10.1007/s00382-018-4582-8>
- 888 Lübbecke JF, Rodriguez-Fonseca B, Richter I et al (2018) Equatorial Atlantic variability—
889 Modes, mechanisms, and global teleconnections. *Wiley Interdisciplinary Reviews-Climate Change* 9:e527. <https://doi.org/10.1002/wcc.527>
- 891 Marchal E, Picaut J (1977) Répartition et abondance évaluées par échantillonnage des
892 poissons du plateau ivoiro-ghanéen en relation avec les upwellings locaux. *Journal de Recherche Océanographique* 2:39-58.
- 894 Marchesiello P, Estrade P (2010) Upwelling limitation by onshore geostrophic flow. *Journal of Marine Research* 68:37-62. <https://doi.org/10.1357/002224010793079004>
- 896 Martins MS, Stammer D (2022) Interannual variability of the Congo River plume-induced sea
897 surface salinity. *Remote Sensing* 14:1013. <https://doi.org/10.3390/rs14041013>
- 898 Menkes CE, Kennan SC, Flament P et al (2002) A whirling ecosystem in the equatorial Atlantic.
899 *Geophysical Research Letters* 29:1553. <https://doi.org/10.1029/2001gl014576>
- 900 Merle J (1980) Seasonal Heat-Budget in the Equatorial Atlantic-Ocean. *Journal of Physical Oceanography* 10:464-469. [https://doi.org/10.1175/1520-0485\(1980\)010<0464:Shbite>2.0.Co;2](https://doi.org/10.1175/1520-0485(1980)010<0464:Shbite>2.0.Co;2)
- 903 Monger B, McClain C, Murtugudde R (1997) Seasonal phytoplankton dynamics in the eastern
904 tropical Atlantic. *Journal of Geophysical Research-Oceans* 102:12389-12411. <https://doi.org/10.1029/96jc03982>
- 906 Moore D, Hisard P, McCreary J et al (1978) Equatorial adjustment in the eastern Atlantic.
907 *Geophysical Research Letters* 5:637-640. <https://doi.org/10.1029/GL005i008p00637>
- 908 Moum JN, Hughes KG, Shroyer EL et al (2022) Deep Cycle Turbulence in Atlantic and Pacific
909 Cold Tongues. *Geophysical Research Letters* 49:e2021GL097345. <https://doi.org/10.1029/2021GL097345>
- 911 Moum JN, Lien RC, Perlin A et al (2009) Sea surface cooling at the Equator by subsurface mixing
912 in tropical instability waves. *Nature Geoscience* 2:761-765. <https://doi.org/10.1038/Ngeo657>
- 913



- 914 Nnamchi HC, Li JP, Kucharski F et al (2015) Thermodynamic controls of the Atlantic Nino.
915 Nature Communications 6:8895. <https://doi.org/10.1038/ncomms9895>
- 916 Okumura Y, Xie SP (2006) Some overlooked features of tropical Atlantic climate leading to a
917 new Nino-like phenomenon. *Journal of Climate* 19:5859-5874. <https://doi.org/10.1175/Jcli3928.1>
- 918
- 919 Oeschies A, Brandt P, Stramma L et al (2018) Drivers and mechanisms of ocean deoxygenation.
920 *Nature Geoscience* 11:467-473. <https://doi.org/10.1038/s41561-018-0152-2>
- 921 Ostrowski M, da Silva JCB, Bazik-Sangolay B (2009) The response of sound scatterers to El
922 Niño- and La Niña-like oceanographic regimes in the southeastern Atlantic. *Ices Journal*
923 *of Marine Science* 66:1063-1072. <https://doi.org/10.1093/icesjms/fsp102>
- 924 Oudot C, Morin P (1987) The distribution of nutrients in the equatorial Atlantic: relation to
925 physical processes and phytoplankton biomass. *Oceanologica Acta Proceedings*
926 *International Symposium on Equatorial Vertical Motion, 6–10 May 1985, Paris*:121-
927 130.
- 928 Perez RC, Hormann V, Lumpkin R et al (2014) Mean meridional currents in the central and
929 eastern equatorial Atlantic. *Climate Dynamics* 43:2943-2962. <https://doi.org/10.1007/s00382-013-1968-5>
- 930
- 931 Perlin A, Moum JN, Klymak JM (2005) Response of the bottom boundary layer over a sloping
932 shelf to variations in alongshore wind. *Journal of Geophysical Research-Oceans*
933 110:C10S09. <https://doi.org/10.1029/2004jc002500>
- 934 Philander SGH, Pacanowski RC (1981) Response of equatorial oceans to periodic forcing.
935 *Journal of Geophysical Research-Oceans and Atmospheres* 86:1903-1916. <https://doi.org/10.1029/Jc086ic03p01903>
- 936
- 937 Philander SGH, Pacanowski RC (1986) A model of the seasonal cycle in the tropical Atlantic-
938 Ocean. *Journal of Geophysical Research-Oceans* 91:14192-14206. <https://doi.org/10.1029/JC091iC12p14192>
- 939
- 940 Picaut J (1983) Propagation of the Seasonal Upwelling in the Eastern Equatorial Atlantic.
941 *Journal of Physical Oceanography* 13:18-37. [https://doi.org/10.1175/1520-0485\(1983\)013<0018:Potsui>2.0.Co;2](https://doi.org/10.1175/1520-0485(1983)013<0018:Potsui>2.0.Co;2)
- 942
- 943 Polo I, Lazar A, Rodriguez-Fonseca B et al (2008) Oceanic Kelvin waves and tropical Atlantic
944 intraseasonal variability: 1. Kelvin wave characterization. *Journal of Geophysical*
945 *Research-Oceans* 113:C07009. <https://doi.org/10.1029/2007jc004495>
- 946 Prigent A, Imbol Kougue RA, Lübbecke JF et al (2020a) Origin of weakened interannual sea
947 surface temperature variability in the southeastern tropical Atlantic Ocean.
948 *Geophysical Research Letters* 47:e2020GL089348. <https://doi.org/10.1029/2020GL089348>
- 949
- 950 Prigent A, Lübbecke JF, Bayr T et al (2020b) Weakened SST variability in the tropical Atlantic
951 Ocean since 2000. *Climate Dynamics* 54:2731-2744. <https://doi.org/10.1007/s00382-020-05138-0>
- 952
- 953 Rabe B, Schott FA, Köhl A (2008) Mean circulation and variability of the tropical Atlantic during
954 1952-2001 in the GECCO assimilation fields. *Journal of Physical Oceanography* 38:177-
955 192. <https://doi.org/10.1175/2007jpo3541.1>
- 956 Radenac MH, Jouanno J, Tchamabi CC et al (2020) Physical drivers of the nitrate seasonal
957 variability in the Atlantic cold tongue. *Biogeosciences* 17:529-545. <https://doi.org/10.5194/bg-17-529-2020>
- 958
- 959 Richter I, Behera SK, Masumoto Y et al (2010) On the triggering of Benguela Niños: Remote
960 equatorial versus local influences. *Geophysical Research Letters* 37:L20604. <https://doi.org/10.1029/2010gl044461>
- 961



- 962 Roch M, Brandt P, Schmidt S et al (2021) Southeastern tropical Atlantic changing from
963 subtropical to tropical conditions. *Frontiers in Marine Science* 8:748383. <https://doi.org/10.3389/fmars.2021.748383>
964
- 965 Rossi V, Feng M, Pattiaratchi C et al (2013) On the factors influencing the development of
966 sporadic upwelling in the Leeuwin Current system. *Journal of Geophysical Research-*
967 *Oceans* 118:3608-3621. <https://doi.org/10.1002/jgrc.20242>
- 968 Rouault M (2012) Bi-annual intrusion of tropical water in the northern Benguela upwelling.
969 *Geophysical Research Letters* 39:L12606. <https://doi.org/10.1029/2012gl052099>
- 970 Rouault M, Illig S, Bartholomae C et al (2007) Propagation and origin of warm anomalies in the
971 Angola Benguela upwelling system in 2001. *Journal of Marine Systems* 68:473-488.
972 <https://doi.org/10.1016/j.jmarsys.2006.11.010>
- 973 Rouault M, Illig S, Lübbecke JF et al (2018) Origin, development and demise of the 2010-2011
974 Benguela Niño. *Journal of Marine Systems* 188:39-48. <https://doi.org/10.1016/j.jmarsys.2017.07.007>
- 975
- 976 Ruiz-Barradas A, Carton JA, Nigam S (2000) Structure of interannual-to-decadal climate
977 variability in the tropical Atlantic sector. *Journal of Climate* 13:3285-3297. [https://doi.org/10.1175/1520-0442\(2000\)013<3285:Soitdc>2.0.Co;2](https://doi.org/10.1175/1520-0442(2000)013<3285:Soitdc>2.0.Co;2)
978
- 979 Sallee JB, Pellichero V, Akhondas C et al (2021) Summertime increases in upper-ocean
980 stratification and mixed-layer depth. *Nature* 591:592-598. <https://doi.org/10.1038/s41586-021-03303-x>
981
- 982 Schafstall J, Dengler M, Brandt P et al (2010) Tidal-induced mixing and diapycnal nutrient
983 fluxes in the Mauritanian upwelling region. *Journal of Geophysical Research-Oceans*
984 115:C10014. <https://doi.org/10.1029/2009jc005940>
- 985 Schott FA, Fischer J, Stramma L (1998) Transports and pathways of the upper-layer circulation
986 in the western tropical Atlantic. *Journal of Physical Oceanography* 28:1904-1928.
987 [https://doi.org/10.1175/1520-0485\(1998\)028<1904:TAPOTU>2.0.CO;2](https://doi.org/10.1175/1520-0485(1998)028<1904:TAPOTU>2.0.CO;2)
- 988 Schott FA, McCreary JP, Johnson GC (2004) Shallow overturning circulations of the tropical-
989 subtropical oceans. In: Wang C, Xie S-P, Carton JA (eds) *Earth Climate: The Ocean-*
990 *Atmosphere Interaction*. American Geophysical Union, Washington, DC, pp 261-304.
991 <https://doi.org/10.1029/147GM15>
- 992 Servain J, Picaut J, Merle J (1982) Evidence of Remote Forcing in the Equatorial Atlantic-Ocean.
993 *Journal of Physical Oceanography* 12:457-463. [https://doi.org/10.1175/1520-0485\(1982\)012<0457:Eorfit>2.0.Co;2](https://doi.org/10.1175/1520-0485(1982)012<0457:Eorfit>2.0.Co;2)
994
- 995 Shannon LV, Boyd AJ, Brundrit GB et al (1986) On the Existence of an El-Niño-Type
996 Phenomenon in the Benguela System. *Journal of Marine Research* 44:495-520. <https://doi.org/10.1357/002224086788403105>
997
- 998 Sherman J, Subramaniam A, Gorbunov MY et al (2022) The photophysiological response of
999 nitrogen-limited phytoplankton to episodic nitrogen supply associated with Tropical
1000 Instability Waves in the equatorial Atlantic. *Frontiers in Marine Science* 8:814663.
1001 <https://doi.org/10.3389/fmars.2021.814663>
- 1002 Siegfried L, Schmidt M, Mohrholz V et al (2019) The tropical-subtropical coupling in the
1003 Southeast Atlantic from the perspective of the northern Benguela upwelling system.
1004 *Plos One* 14:e0210083. <https://doi.org/10.1371/journal.pone.0210083>
- 1005 Sohou Z, Koné V, Da-Allada YC et al (2020) Seasonal and inter-annual ONSET Sea Surface
1006 Temperature variability along the northern coast of the Gulf of Guinea. *Regional*
1007 *Studies in Marine Science* 35:101129. <https://doi.org/10.1016/j.rsma.2020.101129>
- 1008 Sowman M, Cardoso P (2010) Small-scale fisheries and food security strategies in countries in
1009 the Benguela Current Large Marine Ecosystem (BCLME) region: Angola, Namibia and



- 1010 South Africa. *Marine Policy* 34:1163-1170. <https://doi.org/10.1016/j.marpol.2010.03.016>
- 1011
- 1012 Tchikalanga P, Dengler M, Brandt P et al (2018) Eastern Boundary Circulation and Hydrography
- 1013 Off Angola: Building Angolan Oceanographic Capacities. *Bulletin of the American*
- 1014 *Meteorological Society* 99:1589-1605. <https://doi.org/10.1175/Bams-D-17-0197.1>
- 1015 Thomsen S, Capet X, Echevin V (2021) Competition between Baroclinic Instability and Ekman
- 1016 Transport under Varying Buoyancy Forcings in Upwelling Systems: An Idealized Analog
- 1017 to the Southern Ocean. *Journal of Physical Oceanography* 51:3347-3364. <https://doi.org/10.1175/Jpo-D-20-0294.1>
- 1018
- 1019 Tokinaga H, Xie SP (2011) Weakening of the equatorial Atlantic cold tongue over the past six
- 1020 decades. *Nature Geoscience* 4:222-226. <https://doi.org/10.1038/Ngeo1078>
- 1021 Toualy E, Kouacou B, Aman A (2022) Influence of Wind and Surface Buoyancy Flux on the
- 1022 Variability of the Oceanic Mixed Layer Depth in the Northern Gulf of Guinea Coastal
- 1023 Upwelling. *Thalassas* 38:599-608. <https://doi.org/10.1007/s41208-021-00358-5>
- 1024 Tuchen FP, Brandt P, Lübbecke JF et al (2022a) Transports and pathways of the tropical AMOC
- 1025 return flow from Argo data and shipboard velocity measurements. *Journal of*
- 1026 *Geophysical Research-Oceans* 127:e2021JC018115. <https://doi.org/10.1029/2021JC018115>
- 1027
- 1028 Tuchen FP, Lübbecke JF, Brandt P et al (2020) Observed transport variability of the Atlantic
- 1029 Subtropical Cells and their connection to tropical sea surface temperature variability.
- 1030 *Journal of Geophysical Research-Oceans* 125:e2020JC016592. <https://doi.org/10.1029/2020JC016592>
- 1031
- 1032 Tuchen FP, Lübbecke JF, Schmidt S et al (2019) The Atlantic Subtropical Cells Inferred from
- 1033 Observations. *Journal of Geophysical Research-Oceans* 124:7591-7605. <https://doi.org/10.1029/2019jc015396>
- 1034
- 1035 Tuchen FP, Perez RC, Foltz GR et al (2022b) Multidecadal intensification of Atlantic tropical
- 1036 instability waves. *Geophysical Research Letters* 49:e2022GL101073. <https://doi.org/10.1029/2022GL101073>
- 1037
- 1038 Voiturier B, Herbland A, Le Borgne R (1982) L'upwelling équatorial de l'Atlantique Est pendant
- 1039 l'Expérience Météorologique Mondiale (PEMG). *Oceanologica Acta* 5:301-314.
- 1040 Wade M, Caniaux G, du Penhoat Y (2011) Variability of the mixed layer heat budget in the
- 1041 eastern equatorial Atlantic during 2005-2007 as inferred using Argo floats. *Journal of*
- 1042 *Geophysical Research-Oceans* 116:C08006. <https://doi.org/10.1029/2010jc006683>
- 1043 Warner SJ, Holmes RM, Hawkins EHM et al (2018) Buoyant gravity currents released from
- 1044 Tropical Instability Waves. *Journal of Physical Oceanography* 48:361-382. <https://doi.org/10.1175/Jpo-D-17-0144.1>
- 1045
- 1046 Weingartner TJ, Weisberg RH (1991) On the Annual Cycle of Equatorial Upwelling in the
- 1047 Central Atlantic-Ocean. *Journal of Physical Oceanography* 21:68-82. [https://doi.org/10.1175/1520-0485\(1991\)021<0068:Otacoe>2.0.Co;2](https://doi.org/10.1175/1520-0485(1991)021<0068:Otacoe>2.0.Co;2)
- 1048
- 1049 Wiafe G, Nyadjro ES (2015) Satellite Observations of Upwelling in the Gulf of Guinea. *Ieee*
- 1050 *Geoscience and Remote Sensing Letters* 12:1066-1070. <https://doi.org/10.1109/Lgrs.2014.2379474>
- 1051
- 1052 Yang H, Lohmann G, Krebs-Kanzow U et al (2020) Poleward Shift of the Major Ocean Gyres
- 1053 Detected in a Warming Climate. *Geophysical Research Letters* 47:e2019GL085868.
- 1054 <https://doi.org/10.1029/2019GL085868>
- 1055 Zeng Z, Brandt P, Lamb KG et al (2021) Three-dimensional numerical simulations of internal
- 1056 tides in the Angolan upwelling region. *Journal of Geophysical Research-Oceans*
- 1057 126:e2020JC016460. <https://doi.org/10.1029/2020JC016460>